The vibronically-resolved emission spectrum of disulfur monoxide (S_2O): An algebraic calculation and quantitative interpretation of Franck–Condon transition intensities

T. Müller and P. H. Vaccaro
Department of Chemistry, Yale University, New Haven, Connecticut 06520-8107

F. Pérez-Bernal[a] and F. Iachello[b]
Center for Theoretical Physics, Yale University, New Haven, Connecticut 06520-8120

(Received 28 April 1999; accepted 18 June 1999)

Emission spectra obtained from jet-cooled disulfur monoxide (S_2O) molecules have been interpreted by means of a novel Lie algebraic formalism that makes possible the facile evaluation of multidimensional Franck–Condon factors. Fluorescence accompanying selective excitation of isolated vibronic bands in the S_2O $\tilde{C}\ ^1A' \leftarrow \tilde{X}\ ^1A'(\pi^* \leftarrow \pi)$ absorption system has been dispersed under moderate spectral resolution, allowing assignment of ground state levels possessing up to 20 quanta of vibration in the ν_2 S–S stretching mode [$E_{\mathrm{vib}}(\tilde{X}) \leqslant 13\,900\ \mathrm{cm}^{-1}$]. Aside from providing a rigorous and economical description for the inherently anharmonic nature of highly-excited polyatomic species, our algebraic approach enables quantitative information on molecular wavefunctions to be extracted directly from spectroscopic data. The emerging picture of S_2O vibrational dynamics suggests that the $\tilde{X}\ ^1A'$ potential surface is substantially more ''local'' in character than the $\tilde{C}\ ^1A'$ manifold. While the observed pattern of $\tilde{X}\ ^1A'$ vibrational energies could be reproduced well through use of model Hamiltonians that include only diagonal anharmonicities in the local algebraic basis, successful treatment of the $\tilde{C}\ ^1A'$ state necessitated explicit incorporation of off-diagonal anharmonicities that lead to pervasive mixing of local vibrational character. This disparate behavior is manifest strongly in measured $\tilde{C}-\tilde{X}$ transition strengths, thereby allowing detailed investigations of Franck–Condon intensities to discern the underlying dynamics. Structural parameters deduced from algebraic analyses are in good accord with previous predictions of the change in S_2O geometry accompanying $\pi^* \leftarrow \pi$ excitation. © *1999 American Institute of Physics.* [S0021-9606(99)00635-2]

I. INTRODUCTION

It can justifiably be argued that the ''simple'' Franck–Condon factor represents one of the most useful and pervasive mathematical concepts employed for the study of molecules and their interactions. Nominally defined as the square modulus of the overlap integral between normalized vibrational wavefunctions belonging to distinct potential energy surfaces,[1–3] these quantities appear whenever a ''sudden approximation'' is evoked for the description of molecular phenomena within an adiabatic (Born–Oppenheimer) framework. First introduced in the context of traditional optical spectroscopy, where they provide a quantitative interpretation for vibronic transition intensities,[4] Franck–Condon factors also have been exploited extensively for the theoretical modeling of nonradiative processes, including radiationless relaxation,[5,6] predissociation,[6,7] photodissociation/photoassociation,[6–10] proton-/electron-transfer,[11] inelastic/reactive scattering,[12] and electron-mediated surface desorption.[13] Despite the widespread interest engendered by such a diversity of applications, the calculation of multidimensional Franck–Condon factors for polyatomic species has remained a difficult and specialized task, with most published reports to date relying upon the simplifications afforded by harmonic treatments of nuclear motion. This paper demonstrates a new scheme designed to address many of the limitations and inadequacies ascribed to conventional Franck–Condon analyses. Building upon a computationally expedient algebraic formalism that allows for explicit incorporation of vibrational anharmonicity,[14,15] our methodology provides a facile means for the evaluation of multidimensional overlap integrals and related transition matrix elements. Application of such algebraic treatments to the vibronically-resolved emission spectrum of disulfur monoxide (S_2O) illustrates the ability to extract detailed wavefunction information from experimental data while simultaneously highlighting the unique vibrational dynamics that distinguish the ground and excited electronic potential surfaces of this triatomic system.

While the single bond coordinate required for the specification of (one-dimensional) vibrational motion in diatomic species permits the corresponding Franck–Condon factors to

[a]Present address: Facultad de Física, Universidad de Sevilla, Apartado Postal 1065, 41080 Sevilla, Spain.
[b]Also at: Department of Chemistry, Yale University, New Haven, Connecticut 06520-8107.

be evaluated in a straightforward manner,[16] the multidimensional nature of polyatomic potential surfaces introduces both conceptual and practical complexities. Even if overall molecular symmetry is maintained during a (radiative or nonradiative) transition, traditional descriptions of polyatomic vibrational dynamics demand the use of two distinct sets of collective normal coordinates (i.e., one set for each electronic manifold) which must be interconverted by an essentially linear and orthogonal transformation that reflects their relative orientation and/or displacement.[17] For the calculation of Franck–Condon factors and related quantities, this leads to an unavoidable mixing of normal mode character (i.e., the so-called Duschinsky effect)[17,18] which strictly prohibits the separation of vibrational variables and necessitates the explicit evaluation of multidimensional overlap integrals. Nevertheless, several procedures have been developed for the prediction and interpretation of polyatomic spectral intensities, with the requisite transition matrix elements being computed by a variety of ingenious schemes including coherent-state methods,[19] generating function algorithms,[20] intermediate coordinate transformations,[21] and wavefunction addition theorems.[22] However, all of these efforts have relied upon the canonical harmonic oscillator treatment of vibrational behavior which suffices only for small amplitude displacements from the molecular equilibrium configuration. The validity of this approximation is expected to degrade rapidly in the presence of strong anharmonicity such as that encountered in chemically relevant regimes of extreme vibrational excitation.[23] Although some improvement can theoretically be realized through linear superposition of the harmonic (normal mode) basis, the intractability of the resulting expansions will ultimately limit the utility of this approach. Furthermore, the extension of conventional Franck–Condon analyses to encompass polyatomic transitions involving gross changes in equilibrium geometry (e.g., linear-bent and bound-free transitions) or multiple energy minima on a single potential surface (e.g., unimolecular isomerization and proton-/electron-transfer) has not been demonstrated.

Our Franck–Condon methodology relies upon an algebraic scheme that has been employed extensively for the investigation of rovibrational structure in the ground electronic states of both diatomic and polyatomic species. Commonly referred to as the ''vibron'' model, this approach exploits Lie algebras and their inherent dynamical symmetries in order to establish a comprehensive framework for the description of molecules and their interactions.[14,15] Although most applications to date have been spectroscopic in nature, a variety of chemically important issues have been addressed through extension of the underlying concepts, including the determination of absolute thermodynamic properties for complex molecular systems[24] and the elucidation of inelastic electron–molecule/molecule–molecule scattering events.[25] From the perspective of polyatomic spectroscopy, such algebraic treatments can furnish a simple Dunham-type expression[1,2,26] for the characterization of observed energy level patterns, with an unprecedented economy of parametrization following from (algebraic) correlation of expansion coefficients which precede the various powers and products of rotation–vibration quantum numbers.[14,15,27] The robustness of the vibron scheme is augmented further by explicit incorporation of mechanical anharmonicity into the zero-order molecular Hamiltonian, thereby providing a viable means for interpolating the continuum of vibrational behavior that adjoins the pure local-mode and pure normal-mode limits.[14,28] The ensuing analyses build upon the hitherto unexplored ability to evaluate multidimensional Franck–Condon factors and related quantities through use of vibron-based techniques. These calculations can be implemented in a computationally-efficient operator formalism which starts from algebraic expansions of vibrational wavefunctions, applies transformations commensurate with the different equilibrium geometries of the coupled electronic manifolds, and deduces pertinent matrix elements without the intermediate step of generating spatial eigenfunctions. In particular, judicious selection of the expansion basis eliminates many of the complications inherent to conventional Franck–Condon methods (*vide infra*) and should permit efficient treatment of more difficult situations involving linear-bent transitions, bound-free resonances, and several close-lying energy minima. Aside from extracting detailed structural information, such as the change in equilibrium nuclear configuration upon electronic excitation, the quantitative interpretation of algebraic results can provide an unprecedented glimpse at accompanying changes in unimolecular dynamics as reflected by the magnitude and type of anharmonic coupling that exists among vibrational degrees of freedom.

The present work focuses on vibronically-resolved emission spectra exhibited by transient disulfur monoxide (S_2O) molecules entrained in a rotationally-cold ($T_{rot} \approx 5$ K) supersonic slit-jet expansion. Since the initial report of a new oxide of sulfur by Schenk in 1933,[29] the highly reactive S_2O system has suffered a long history of mistaken identity and muddled spectral interpretation. Erroneous determinations of chemical stoichiometry[30,31] led to several proposed geometries based on a sulfur-to-oxygen ratio of unity.[32] While not the first to contest empirical formulas suggested for Schenk's ''sulfur monoxide,'' [33] the work of Meschi and Myers in the late 1950's employed mass[30] and microwave[31] spectroscopic techniques to prove conclusively the presence of a triatomic S_2O species where the $\tilde{X}\ ^1A'$ ground state potential surface supports an equilibrium configuration that is both unsymmetrical and bent. Subsequent microwave[34] and infrared[32,35–37] measurements have furnished refined $\tilde{X}\ ^1A'$ structural parameters of $r_{so} = 1.4594$ Å, $r_{ss} = 1.8845$ Å, and $\angle \mathrm{SSO} = 118.08°$ with the fundamental vibrational frequencies of 1166.5, 679.1, and 380 cm^{-1} being assigned to the ν_1 (S–O stretching), ν_2 (S–S stretching), and ν_3 (S–S–O bending) degrees of freedom, respectively. *Ab initio* calculations have predicted the existence of at least two other bound S_2O isomers having C_{2v} symmetry,[38,39] however, experimental evidence for these structures, as well as for the accompanying unimolecular isomerization processes, has not been reported to date.

Numerous studies have been conducted on the intense, richly-structured absorption spectrum of S_2O which extends from ~3400 to ~2500 Å.[29,32,40,41] The abrupt disappearance of spontaneous emission[32,41–45] above ~31 200 cm^{-1} and the

diffuse nature of higher-lying bands[46] provide evidence for the onset of predissociation within the pertinent electronically-excited manifold. Based on the essentially parallel nature of resolved rovibronic lines, Hallin, Merer, and Milton[44] established the transition symmetry as $^1A' \leftarrow {}^1A'$ with the excited state designation of $\tilde{C}\ ^1A'$ stemming from similarities drawn by Chiu, *et al.*[45] to the analogous $\pi^* \leftarrow \pi$ system of SO_2. Under the assumption of a fixed 1.50 Å S–O bond length, rotational constants suggested the $\tilde{C}\ ^1A'$ potential surface to support an equilibrium geometry characterized by $r_{ss}=2.14$ Å and $\angle \mathrm{SSO} \approx 109°$.[44] Detailed laser-induced fluorescence (LIF) and optical–optical double resonance (OODR) probes of the $\tilde{C}-\tilde{X}$ resonance have been reported by Tsukiyama and co-workers,[42] with subsequent jet-cooled measurements by Clouthier and Rutherford[43] serving to alleviate the hot-band activity and rovibronic congestion that severely hamper spectral interpretation. Vibrational analyses performed by these authors led to the assignment of 1032, 407, and 253 cm^{-1} as the fundamental frequencies for the $\tilde{C}\ ^1A'$ ν_1 (S–O stretching), ν_2 (S–S stretching), and ν_3 (bending) modes, respectively. By exploiting a seeded free-jet expansion of S_2O molecules ($T_{rot} \approx 1$ K) in conjunction with high-resolution LIF spectroscopy, Zhang, *et al.*[46,47] have examined axis-switching and predissociation effects in the lowest-lying $\tilde{C}-\tilde{X}$ bands, thereby providing refined rotational and vibrational constants ($\nu_2=415.2\ cm^{-1}$) as well as state-specific data regarding collision-free lifetimes. The deduced rates of nonradiative relaxation processes were quantified in terms of a rudimentary one-dimensional tunneling model which established ν_2 as the promoting mode for unimolecular decomposition and predicted a predissociation barrier to reside in the vicinity of the $\tilde{C}\ ^1A'\ \nu_2=6$ level. The experimental and theoretical efforts discussed below build upon these prior investigations of S_2O in order to extract structural and dynamical information encoded in vibronically-resolved $\tilde{C} \rightarrow \tilde{X}$ emission spectra.

II. EXPERIMENTAL TECHNIQUES

Since the basic techniques employed for fluorescence studies of jet-cooled S_2O molecules have been described in previous publications,[46,48] only the most salient experimental features will be repeated here. Tunable ultraviolet radiation was generated by frequency doubling (Inrad Autotracker II; servo-locked BBO crystal) the fundamental output of a high-resolution dye laser (Lambda Physik FL3002E; $<0.035\ cm^{-1}$ spectral bandwidth) which was pumped by the second harmonic of an injection-seeded Nd:YAG system (Spectra Physics GCR-4-20; 20 pps repetition rate, ~8 ns pulse duration). The resulting ~330 nm light was spatially filtered and recollimated to a diameter of 0.4–0.5 cm before passing through brewster-angle windows mounted on the baffled entrance and exit arms of the molecular beam apparatus. The absolute dye laser frequency was calibrated through use of a heated iodine absorption cell[49] and the ultraviolet energy impinging upon the S_2O sample was attenuated to the lowest values consistent with acceptable signal-to-noise ratios.

The requisite S_2O molecules were generated *in situ* by means of a heterogeneous reaction[50] in which the vapor pressure of cooled $SOCl_2$ (~37 Torr at 0 °C)[51] was entrained in ~4.5 atm of helium carrier gas and passed through a heated Pyrex tube (100 °C–150 °C) containing CuS powder suspended in a glass wool matrix. Chemically-inert tubing directed the resulting S_2O/He mixture into a pulsed free-jet source based upon a current-loop actuator capable of producing choke-flow pulses of $\leqslant 60$ μs duration (R. M. Jordan Co. C-211SS; modified for 20 pps operation). The unique ''flow-through'' geometry inherent to this apparatus permitted the highly reactive target molecules to be swept continuously past the nozzle assembly with the rate of flow adjusted manually in order to achieve an optimal balance between surface-mediated production and decomposition of the S_2O species. While preliminary experiments were performed with a circular expansion orifice (0.05 cm diameter),[48] the studies reported below made use of a custom rectangular nozzle aperture of 0.015 cm width and 1.15 cm length.[52] The improved velocity collimation and extended interaction pathlength afforded by this modification enhanced measured signal-to-noise ratios greatly while still maintaining reasonable quenching of internal degrees of freedom ($T_{rot} \approx 5$ K).[52] With the sample chamber evacuated by a liquid nitrogen-baffled 6″ diffusion pump, ambient pressures of $<5 \times 10^{-5}$ Torr, as measured by an uncalibrated ionization gauge, could be maintained under typical 20 pps operating conditions.

The ultraviolet excitation light propagated through the S_2O/He slit-jet expansion ~1 cm downstream from the nozzle orifice in a direction parallel to the major axis of the rectangular aperture and perpendicular to the axis of molecular flow. Identical sets of custom $f/1.0$ imaging optics arranged symmetrically on both sides of the plane defined by intersection of the molecular and laser beams were used to monitor spontaneous emission emerging from the interaction region. Light collected by one of these optical assemblies passed through spectral filters selected to reject stray light and impinged upon the photocathode of an ambient (~25 °C) photomultiplier tube (Hamamatsu R331). The resulting photocurrent was preamplified and directed to a CAMAC-based gated integrator that enabled the total fluorescence intensity to be recorded as a function of excitation wavelength. Once tuned to a selected rovibronic line of the S_2O $\tilde{C}\ ^1A'-\tilde{X}\ ^1A'$ system, the relative stability of target molecule production could be assessed readily by monitoring the magnitude of this undispersed LIF signal.

Spontaneous emission collected by the remaining optical assembly was directed through a 0.5 m Ebert scanning monochromator (Jarrell–Ash 82-020; used in first-order) which contained an 1180 groove/mm diffraction grating blazed for 400 nm radiation. Monochromator scans were performed at instrumental slit widths of 50, 200, and 250 μm thereby yielding an effective resolution of 0.8, 3.2 and 4.0 Å, respectively. Resolved fluorescence was detected by an ambient (~25 °C) photomultiplier tube (Hamamatsu R666) having uniform radiant sensitivity over the near-ultraviolet and visible regions of the spectrum (specified photocathode radiant sensitivity of 70 ± 5 mA/W over 4000–8000 Å range,

dropping to ~ 60 mA/W at 3400 Å).[53] The resulting photocurrent was preamplified, directed to a gated integrator, and recorded as a function of dispersed wavelength with active (shot-by-shot) amplitude stabilization following from normalization of the integrated signal by the corresponding total (undispersed) fluorescence intensity. All data acquisition functions were controlled by a custom software package running in a personal computer environment; however, the subsequent processing and analysis of data were performed on RISC workstations. Atomic emission lamps, in conjunction with the known frequency of the excitation laser, were used to calibrate the wavelength scale of the monochromator. The nonuniform spectral sensitivity of the detection train was corrected by employing the calibrated output of a quartz halogen lamp (Eppley Laboratory) that was inserted directly into the S_2O interaction region while the accompanying polarization dependence (i.e., stemming primarily from the polarization-selective diffraction efficiency of the monochromator) necessitated additional polarized fluorescence measurements to derive appropriate adjustment factors. As a result of such procedures, reported ground state vibrational energies are believed to be accurate to better than ± 5 cm^{-1} and the relative emission strengths of vibronically-resolved features derived from a given excitation line should exhibit uncertainties of less than $\pm 5\%$. Repeated dispersed fluorescence experiments performed on a selected subset of $\tilde{C}\ ^1A'-\tilde{X}\ ^1A'$ absorption bands have corroborated the validity of these error estimates.

III. SURVEY OF EXPERIMENTAL RESULTS

Resolved S_2O fluorescence measurements were performed by tuning the frequency of the incident ultraviolet radiation into resonance with the prominent $^qR_0(1)$ rotational line of isolated vibronic features in the jet-cooled $\tilde{C}\ ^1A'-\tilde{X}\ ^1A'$ absorption system. Extensive LIF probes, as well as recorded emission patterns, permitted the ten peaks selected for the present investigation to be assigned unambiguously as the 0_0^0 (29 688.2 cm^{-1}), 2_0^1 (30 098.8 cm^{-1}), 2_0^2 (30 505.6 cm^{-1}), 2_0^3 (30 908.5 cm^{-1}), 2_0^4 (31 307.2 cm^{-1}), 1_0^1 (30 721.8 cm^{-1}), 3_0^1 (30 721.8 cm^{-1}), $1_0^1 2_1^1$ (29 942.0 cm^{-1}), $2_0^1 3_0^1$ (30 446.7 cm^{-1}), and $2_0^2 3_0^1$ (30 755.1 cm^{-1}) bands where values in parentheses denote the corresponding excitation wavenumbers. Given the dominance of type-*a* selection rules,[44,46] vibronic transitions in the resulting dispersed fluorescence spectra should nominally consist of two resonances that terminate on the $1_{0,1}$ and $3_{0,3}$ rotational levels of a particular $\tilde{X}\ ^1A'$ vibrational state. High-resolution stimulated emission pumping (SEP) studies[54] have shown such rotational lines to be separated by ~1.6 cm^{-1}, thereby prohibiting their direct observation under monochromator-limited resolution. Previous $\tilde{C}-\tilde{X}$ rotational analyses have documented the existence of a minute axis-switching effect that induces *b*-polarized transition character;[46] however, such phenomena are not expected to introduce significant perturbations for vibronically-resolved spectra acquired in a rotationally-cold molecular beam environment. In particular, the $\leqslant 2°$ axis-switching angles deduced for the lowest-lying

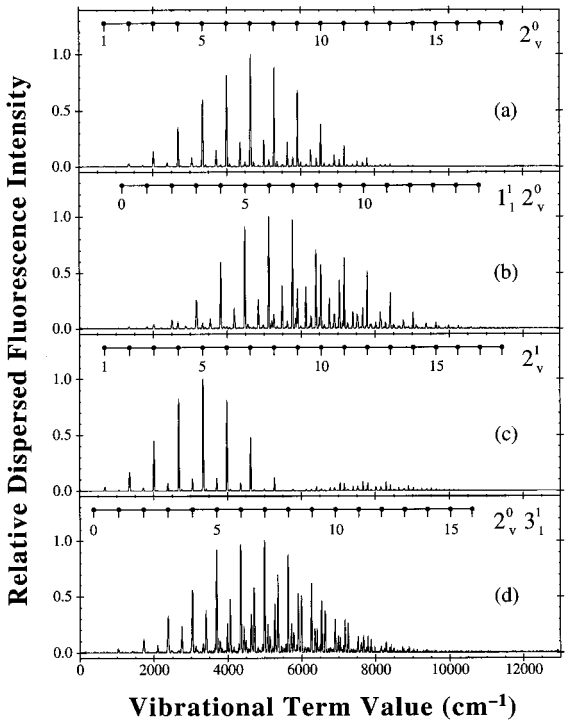

FIG. 1. Experimental emission spectra for the S_2O $\tilde{C}-\tilde{X}$ system. The depicted dispersed fluorescence spectra were acquired under supersonic slit-jet conditions ($T_{rot} \approx 5$ K) by selective excitation of the (a) 0_0^0(29 688.2 cm^{-1}), (b) 1_0^1(30 721.8 cm^{-1}), (c) 2_0^1(30 098.8 cm^{-1}), and (d) 3_0^1(29 942.0 cm^{-1}) bands in the S_2O $\tilde{C}\ ^1A'-\tilde{X}\ ^1A'$ absorption system where the values in parentheses denote the location of targeted $^qR_0(1)$ rotational lines. Isolated emission features exhibit full-widths of 10–20 cm^{-1} which are commensurate with the monochromator-limited resolution achieved in these experiments. The vibronic assignments in each panel highlight prominent ground state progressions built upon overtones of the ν_2 S–S stretching vibration where the number of quanta in the ν_1 S–O stretching and ν_3 S–S–O bending modes remains unchanged upon $\tilde{C} \rightarrow \tilde{X}$ transition.

members of the $2_0^{v'}$ progression have been shown to introduce only slight perturbations in the intensities of rotational features recorded under typical jet-cooled conditions.

Figure 1 illustrates a portion of the dispersed fluorescence data obtained through selective excitation of the (a) 0_0^0 (origin), (b) 1_0^1, (c) 2_0^1, and (d) 3_0^1 bands in the $\tilde{C}-\tilde{X}$ system. These results are in good accord with those reported in our preliminary analysis of the S_2O emission spectrum;[48] however, the present experimental efforts are much broader in scope and quality, reflecting significant improvements in resolution, sensitivity, and calibration. Since the optical detection efficiency has been corrected for constant radiant sensitivity, the intensity information exhibited by Fig. 1 and utilized for all subsequent Franck–Condon calculations is directly proportional to spectral irradiance. Each dispersed fluorescence trace contains ~100 resonances, leading to a total of ~1000 calibrated emission intensities and transition frequencies for the ten selected excitation lines. The resulting compilation of 240 distinct $\tilde{X}\ ^1A'$ vibrational levels (cf. Table I) spans ground state energies extending from the zero-point to approximately 14 000 cm^{-1} and accesses eigenstates

TABLE I. Vibrational term values for the $\tilde{X}\ ^1A'$ state of S_2O. Measured energies for the $\tilde{X}\ ^1A'$ potential surface were obtained from roughly 25 dispersed fluorescence spectra which resulted from selective excitation of single rotational lines in ten distinct vibronic bands of the jet-cooled $\tilde{C}\ ^1A'-\tilde{X}\ ^1A'$ absorption system. Although instrumental resolution varied between 0.8 and 4.0 Å, reported vibrational terms are estimated to have uncertainties of ± 5 cm^{-1}. The calculated energies follow from diagonalization of an optimized vibron Hamiltonian for the ground state, thereby yielding a root-mean-square deviation from experimental values of 5.7 cm^{-1}. Vibrational assignments were generated by means of an iterative procedure which started from known fundamental frequencies and a minimal algebraic description, the later being refined successively upon (incremental) inclusion of data derived from higher-lying vibrational eigenstates.

$v_1\ v_2\ v_3$	Measured term energy	Calculated term energy	Residual	$v_1\ v_2\ v_3$	Measured term energy	Calculated term energy	Residual	$v_1\ v_2\ v_3$	Measured term energy	Calculated term energy	Residual
0 0 1	377.4	381.6	−4.2	1 6 4	6588.7	6586.6	2.1	2 12 0	9996.7	10 002.5	−5.8
0 1 0	680.2	676.4	3.9	0 9 2	6633.7	6629.6	4.1	0 14 3	10 070.2	10 077.0	−6.8
0 0 2	754.9	762.9	−8.1	2 6 1	6645.1	6639.0	6.1	2 11 2	10 088.4	10 096.7	−8.2
0 1 1	1056.1	1054.8	1.3	0 8 4	6718.3	6716.5	1.7	1 14 0	10 118.1	10 118.7	−0.6
1 0 0	1158.1	1151.2	6.8	1 8 1	6775.5	6772.0	3.4	2 10 4	10 198.7	10 192.3	6.4
0 2 0	1352.1	1347.9	4.2	1 7 3	6862.9	6859.1	3.8	0 16 0	10 230.7	10 235.3	−4.6
0 1 2	1430.4	1433.0	−2.7	0 10 1	6905.9	6901.6	4.3	3 10 1	10 249.0	10 239.5	9.4
1 0 1	1535.8	1530.6	5.2	2 7 0	6921.3	6914.1	7.1	2 9 6	10 291.5	10 289.3	2.1
0 2 1	1722.7	1723.4	−0.6	0 9 3	6992.5	6987.9	4.6	0 15 2	10 336.3	10 331.7	4.6
0 1 3	1809.8	1811.0	−1.2	2 6 2	7006.7	6999.4	7.3	2 12 1	10 344.3	10 351.6	−7.3
1 1 0	1838.7	1833.2	5.5	1 9 0	7046.7	7043.7	3.0	4 9 0	10 376.9	10 383.8	−6.9
0 3 0	2012.5	2014.6	−2.2	1 8 2	7133.8	7130.3	3.4	0 14 4	10 431.0	10 427.4	3.6
0 2 2	2094.5	2098.6	−4.1	0 11 0	7172.5	7172.3	0.2	1 14 1	10 460.0	10 467.3	−7.3
1 1 1	2211.5	2209.4	2.1	1 7 4	7219.3	7219.1	0.2	3 11 0	10 490.9	10 493.6	−2.7
0 3 1	2384.2	2387.2	−3.1	0 10 2	7257.0	7258.3	−1.3	2 10 5	10 548.0	10 544.1	3.9
0 2 3	2472.9	2473.6	−0.7	2 7 1	7274.8	7272.5	2.3	1 13 3	10 571.5	10 562.4	9.1
1 2 0	2505.7	2507.6	−1.9	0 9 4	7347.1	7346.1	1.0	0 16 1	10 583.8	10 583.8	0.0
1 1 2	2585.8	2585.4	0.4	1 9 1	7404.2	7400.2	4.0	2 13 0	10 595.9	10 605.2	−9.4
0 4 0	2676.1	2676.5	−0.3	1 8 3	7488.3	7488.4	−0.1	0 15 3	10 686.9	10 681.0	5.9
0 3 2	2757.5	2759.7	−2.1	0 11 1	7525.0	7527.4	−2.4	1 15 0	10 718.4	10 720.1	−1.6
1 2 1	2877.5	2880.9	−3.4	2 8 0	7544.9	7543.2	1.6	4 9 1	10 752.5	10 733.7	18.8
2 1 0	2980.9	2980.8	0.1	0 10 3	7620.1	7614.9	5.2	0 14 5	10 775.9	10 777.6	−1.6
0 4 1	3049.0	3046.4	2.6	2 7 2	7633.5	7630.7	2.8	2 11 4	10 796.6	10 797.5	−0.9
0 3 3	3124.5	3131.8	−7.4	1 10 0	7673.3	7668.5	4.8	0 17 0	10 827.3	10 832.9	−5.6
1 3 0	3171.9	3174.9	−2.9	1 9 2	7755.6	7756.5	−0.9	3 11 1	10 853.7	10 842.2	11.6
1 2 2	3248.6	3253.9	−5.3	0 12 0	7793.6	7794.8	−1.2	2 10 6	10 889.1	10 895.7	−6.5
0 5 0	3332.8	3333.4	−0.6	18 4	7850.8	7846.4	4.4	1 13 4	10 916.8	10 911.9	4.9
0 4 2	3419.1	3416.1	3.0	0 11 2	7883.9	7882.4	1.5	0 16 2	10 938.2	10 932.1	6.0
0 3 4	3498.7	3503.7	−5.1	2 8 1	7904.1	7899.5	4.7	4 10 0	10 976.3	10 986.1	−9.8
1 3 1	3547.7	3545.3	2.4	2 7 3	7984.1	7988.7	−4.6	0 15 4	11 027.6	11 030.2	−2.6
1 2 3	3642.1	3626.7	15.5	1 10 1	8023.0	8023.1	−0.1	1 15 1	11 056.7	11 067.4	−10.7
2 2 0	3659.1	3658.1	1.0	3 7 0	8039.6	8041.1	−1.5	4 9 2	11 082.6	11 083.5	−0.9
0 5 1	3701.1	3700.8	0.3	1 9 3	8111.3	8112.7	−1.3	0 14 6	11 140.0	11 127.5	12.5
0 4 3	3785.9	3785.6	0.3	0 12 1	8149.5	8148.4	1.1	1 14 3	11 168.6	11 164.1	4.5
1 4 0	3834.1	3835.3	−1.1	2 9 0	8170.0	8166.1	3.9	0 17 1	11 181.3	11 180.4	0.9
1 3 2	3911.8	3915.5	−3.7	0 11 3	8232.2	8237.3	−5.0	3 11 2	11 191.3	11 190.6	0.7
0 6 0	3983.1	3985.5	−2.3	2 8 2	8257.7	8255.6	2.1	1 13 5	11 256.9	11 261.2	−4.3
0 5 2	4069.9	4068.0	1.8	1 11 0	8289.5	8288.2	1.3	0 16 3	11 282.7	11 280.4	2.3
0 4 4	4158.4	4154.9	3.4	1 10 2	8374.2	8377.6	−3.4	1 16 0	11 315.5	11 317.2	−1.8
1 4 1	4202.9	4203.0	−0.1	3 7 1	8397.8	8397.3	0.5	0 15 5	11 370.8	11 379.2	−8.4
1 3 3	4284.6	4285.4	−0.8	0 13 0	8415.3	8412.4	2.9	2 12 4	11 391.0	11 398.3	−7.3
2 3 0	4309.2	4325.9	−16.7	1 9 4	8456.4	8468.6	−12.2	0 18 0	11 420.1	11 425.6	−5.5
0 6 1	4349.6	4350.5	−1.0	0 12 2	8498.2	8501.8	−3.6	3 12 1	11 456.0	11 440.2	15.8
0 5 3	4433.6	4435.0	−1.4	2 9 1	8524.5	8520.4	4.0	1 14 4	11 520.7	11 512.3	8.4
1 5 0	4489.0	4489.0	−0.0	0 11 4	8590.8	8591.9	−1.1	0 17 2	11 532.6	11 527.8	4.7
1 4 2	4568.7	4570.5	−1.8	2 8 3	8612.7	8611.5	1.2	2 14 1	11 565.7	11 550.3	15.4
0 7 0	4629.0	4632.7	−3.7	1 11 1	8638.8	8641.1	−2.3	0 16 4	11 620.2	11 628.5	−8.3
0 6 2	4717.1	4715.3	1.7	3 8 0	8663.5	8663.7	−0.2	2 13 3	11 651.2	11 648.0	3.2
0 5 4	4802.0	4801.8	0.3	1 10 3	8727.8	8732.0	−4.2	1 16 1	11 670.0	11 663.5	6.5
1 5 1	4855.1	4854.2	0.9	0 13 1	8764.4	8764.5	−0.1	1 15 3	11 761.0	11 761.8	−0.8
1 4 3	4938.0	4937.8	0.2	2 10 0	8786.8	8783.4	3.4	0 18 1	11 780.0	11 772.2	7.8
2 4 0	4977.4	4984.8	−7.4	0 12 3	8849.6	8855.1	−5.5	2 15 0	11 792.2	11 799.0	−6.8
0 7 1	4994.9	4995.5	−0.5	2 9 2	8872.4	8874.5	−2.2	1 14 5	11 862.0	11 860.3	1.7
0 6 3	5082.5	5080.0	2.5	1 12 0	8902.3	8903.0	−0.7	0 17 3	11 877.0	11 875.1	1.9
1 6 0	5137.5	5136.5	1.0	1 11 2	8991.9	8993.9	−2.0	1 17 0	11 910.7	11 910.4	0.3
1 5 2	5219.1	5219.2	−0.1	0 14 0	9030.2	9025.0	5.2	0 19 0	12 011.5	12 013.2	−1.7
0 8 0	5271.9	5275.0	−3.1	1 10 4	9076.8	9086.1	−9.4	0 18 2	12 113.3	12 118.7	−5.4
1 4 4	5303.6	5304.9	−1.3	0 13 2	9109.9	9116.5	−6.6	2 15 1	12 155.5	12 144.1	11.3
2 4 1	5343.1	5350.3	−7.3	2 10 1	9133.7	9135.8	−2.1	1 17 1	12 258.5	12 255.6	2.9

TABLE I. (*Continued.*)

$\nu_1\ \nu_2\ \nu_3$	Measured term energy	Calculated term energy	Residual	$\nu_1\ \nu_2\ \nu_3$	Measured term energy	Calculated term energy	Residual	$\nu_1\ \nu_2\ \nu_3$	Measured term energy	Calculated term energy	Residual
0 7 2	5356.6	5358.1	−1.5	2 9 3	9229.3	9228.5	0.8	0 19 1	12 353.8	12 359.0	−5.2
0 6 4	5449.8	5444.4	5.5	1 12 1	9251.6	9254.3	−2.7	3 13 2	12 374.1	12 379.6	−5.5
1 6 1	5501.5	5499.3	2.2	3 9 0	9280.8	9279.5	1.2	2 16 0	12 399.5	12 390.7	8.8
1 5 3	5581.8	5584.0	−2.2	1 11 3	9335.4	9346.6	−11.2	1 18 0	12 498.4	12 499.7	−1.3
0 8 1	5632.6	5635.6	−3.0	0 14 1	9374.8	9375.8	−1.0	0 20 0	12 599.9	12 595.8	4.1
2 4 2	5707.1	5715.7	−8.6	2 11 0	9395.5	9395.3	0.2	0 19 2	12 708.0	12 704.8	3.2
0 7 3	5726.5	5720.5	6.0	0 13 3	9464.2	9468.4	−4.1	2 16 1	12 739.6	12 734.8	4.8
1 7 0	5780.3	5778.0	2.3	2 10 2	9481.4	9488.1	−6.7	2 15 3	12 832.8	12 834.2	−1.4
1 6 2	5863.1	5861.9	1.1	1 13 0	9509.9	9513.1	−3.2	1 18 1	12 852.6	12 844.1	8.5
0 9 0	5910.1	5912.3	−2.2	0 12 5	9560.9	9561.1	−0.2	0 20 1	12 939.9	12 941.0	−1.1
1 5 4	5948.7	5948.6	0.1	0 12 2	9596.0	9605.6	−9.5	3 14 2	12 960.7	12 968.8	−8.1
0 8 2	5996.0	5996.1	−0.1	0 15 0	9642.0	9632.6	9.4	2 16 2	13 077.0	13 078.7	−1.8
0 7 4	6090.2	6082.6	7.6	1 11 4	9689.7	9699.0	−9.4	1 19 0	13 099.4	13 085.2	14.2
1 7 1	6141.4	6138.5	2.9	0 14 2	9723.0	9726.5	−3.4	1 18 2	13 187.5	13 188.4	−0.8
1 6 3	6227.4	6224.4	3.0	2 11 1	9738.1	9746.1	−8.0	2 17 1	13 319.3	13 332.5	−3.2
0 9 1	6272.7	6271.0	1.7	4 8 0	9768.0	9775.0	−6.9	2 16 3	13 414.1	13 422.6	−8.5
2 6 0	6282.0	6278.4	3.6	2 10 3	9830.2	9840.3	−10.1	1 19 1	13 436.0	13 428.9	7.2
0 8 3	6361.1	6356.4	4.7	1 13 1	9855.5	9863.0	−7.5	2 18 0	13 555.7	13 565.4	−9.7
1 8 0	6416.4	6413.6	2.8	3 10 0	9890.6	9889.3	1.3	1 20 0	13 650.0	13 667.3	−17.3
1 7 2	6503.3	6498.9	4.4	2 9 5	9943.8	9935.9	7.9	2 17 2	13 682.2	13 665.5	16.7
0 10 0	6544.6	6544.8	−0.1	0 15 1	9982.8	9982.2	0.6	3 15 3	13 892.8	13 898.0	−5.2

possessing up to 4, 20, and 5 quanta, respectively, in the ν_1, ν_2, and ν_3 modes. Although effective monochromator resolution varied considerably over this range, experiments have shown the reproducibility in measured peak positions to be better than $\pm 5\ \mathrm{cm}^{-1}$.

As demonstrated by the vibronic assignments appearing in Fig. 1, the S_2O fluorescence data are dominated by extensive progressions built upon the ν_2 S–S stretching mode. This observation, as well as the monotonic increase in $2_0^{v'}$ absorption strength noted over the range of $0 \leqslant v' \leqslant 10$,[41] reflects the substantial change in S–S bond length that accompanies the $\pi^* \leftarrow \pi$ electron promotion. The most intense transitions in each spectrum are found to conserve v_1 and v_3 quantum numbers with the highlighted (a) 2_v^0, (b) $1_1^1 2_v^0$, (c) 2_v^1, and (d) $2_v^0 3_1^1$ features displaying vibronically-resolved emission envelopes which contain internal nodes equal in number to that of ν_2 quanta in the $\tilde{C}\ ^1A'$ state. This conclusion is reinforced dramatically by results obtained through excitation of higher-lying $\tilde{C}$–$\tilde{X}$ bands (e.g., $2_0^{v'}$ with $v' \geqslant 2$), thereby leading to a situation reminiscent of that expected from the application of simple Franck–Condon arguments to a pseudodiatomic S–(SO) species.[1] Attempts to quantify these assertions by modeling the measured ν_2 vibrational structure for each electronic manifold in terms of displaced, one-dimensional Morse oscillators and numerically evaluating Franck–Condon factors from the corresponding wavefunctions proved to be unsatisfactory. Moderate agreement was obtained for the lowest-lying members of progressions involving *exclusively* the S–S stretching coordinate (viz. $2_v^{v'}$); however, the ability of this rudimentary treatment to reproduce experimental intensities deteriorated rapidly with increasing ν_2 vibrational energy content. While such behavior might be taken as evidence for ground state intramolecular vibrational redistribution (IVR)[55] whereby $\tilde{C}$–$\tilde{X}$ transition probability is distributed over neighboring $\tilde{X}\ ^1A'$ eigenstates, the ensuing vibron analyses will attribute its manifestation to the distinct (nonlocal) vibrational dynamics supported by the $\tilde{C}\ ^1A'$ potential surface.

IV. LIE ALGEBRAIC ANALYSES

A. Lie algebraic realization of the morse oscillator

Since their mathematical inception in 1893,[56] Lie algebras have been exploited extensively for the simplified description of complex physical systems. The Lie algebraic generation of spectral information was demonstrated for nuclear physics in 1974[57] with the resulting interacting boson model (IBM) representing a now-standard framework for the quantitative interpretation of nuclear structure.[58] The underlying IBM methodology was extended subsequently to formulate the molecular vibron model[59] in which molecules are treated as coupled assemblies of quantized (bosonic) excitations that are commonly referred to as vibrons.[14,15] The energy eigenvalues and eigenfunctions for the system are obtained from an algebraic Hamiltonian, thereby providing the requisite ingredients for the calculations of transition frequencies and intensities. While the vibron scheme can provide capabilities that complement those afforded by more traditional approaches to molecular structure and dynamics, its most important advantage stems from the anharmonic nature of the fundamental building blocks (the vibrons). Vibrational anharmonicity can thus be incorporated explicitly from the onset, leading to economical parametrization and rapid convergence of expansions used to describe polyatomic en-

ergy levels and wavefunctions.[14,15] Such characteristics are of paramount importance for chemically-relevant situations involving highly vibrationally-excited molecules and complicated potential energy hypersurfaces. This general scheme can be implemented in a variety of different forms that reflect the essential properties of a particular problem. The simplest case, corresponding to a $U(2)$ Lie algebraic treatment,[14,15] employs one-dimensional basis functions which associate the elementary vibrons with excitations of either Morse[60,61] (for stretching) or Pöschl–Teller[62,63] (for bending) potentials. For inherently two-dimensional situations (e.g., the doubly-degenerate bending modes of linear polyatomics), a more sophisticated treatment can be formulated in terms of a $U(3)$ framework.[64] Finally, in cases where the separation of rotational and vibrational degrees of freedom is compromised, a full three-dimensional vibron model can be built upon the Lie algebra $U(4)$.[59]

The ensuing analyses of vibronically-resolved S_2O emission data build upon a coupled $U(2)$ framework that enables the vibrational Hamiltonian for each electronic manifold to be formulated in terms of bosonic creation and annihilation operators which describe interacting anharmonic degrees of freedom (i.e., vibrons). The origin of this approach can be traced to the isomorphism that exists between the unitary Lie algebra $U(2)$ and the energy spectrum of a one-dimensional Morse oscillator[14] defined by the potential function $V(x) = D[1-e^{-\beta x}]^2$ where D denotes the dissociation energy and β represents the range parameter. In particular, a one-to-one correspondence can be established between eigenstates of the Morse–Schrödinger equation, $h|\varphi\rangle = \varepsilon|\varphi\rangle$ with $h = p^2/2m + V(x)$, and the representations of $U(2)$, $|N,v\rangle$, the latter being characterized by two quantum numbers which specify the total number of bound levels, $1+N/2$ or $1+(N-1)/2$ (N even or N odd), and the vibrational index, v, such that $v = 0,1...N/2$ or $(N-1)/2$. When recast in the $U(2)$ basis, the Morse Hamiltonian assumes the simple form $h = \varepsilon_0 + AC$ where ε_0 and A signify constant modeling parameters while C is related to the invariant quadratic Casimir operator $\mathcal{C}$ of the subalgebra $O(2)$ [with eigenvalues $m^2 = (N-2v)^2$] by means of:[65,66]

$$C = \frac{1}{4N}(N^2 - \mathcal{C}). \tag{1}$$

With this definition, the eigenvalues of h in the $U(2)$ representation can be written as $\varepsilon = \varepsilon_0 + A(v - v^2/N)$ which, upon introduction of the substitutions $A = \omega_e$ and $N = \omega_e/\omega_e x_e$, yields the more conventional spectroscopic expression:

$$\varepsilon = \varepsilon_0 + \omega_e v - \omega_e x_e v^2, \tag{2}$$

where ω_e and $\omega_e x_e$ denote the traditional frequency and anharmonicity (in units of cm^{-1}) for the one-dimensional Morse oscillator of reduced mass μ. In turn, these parameters can be related to the structural constants which appear in the corresponding potential function, $V(x)$:[1,14]

$$\omega_e = \frac{\beta}{2\pi c}\sqrt{\frac{2D}{\mu}}, \quad \omega_e x_e = \frac{\hbar\beta^2}{4\pi c\mu}. \tag{3}$$

The algebraic Morse representation can serve as an anharmonic expansion basis for describing more complex interactions as a power series in operator C:

$$h = \varepsilon_0 + \sum_k A^{(k)} C^k, \tag{4}$$

and can be exploited to construct model Hamiltonians for assemblies of coupled (anharmonic) oscillators.[14,15] Similar algebraic developments can be demonstrated for the one-dimensional Pöschl–Teller potential which displays bound states isospectral to those of the Morse form.

B. Vibrational frequencies of polyatomic molecules

The $U(2)$ algebraic scheme enables the vibrational structure of a polyatomic system to be treated as an assembly of n coupled Morse (and/or Pöschl–Teller) oscillators,[14,15] where n equals the number of vibrational degrees of freedom. The resulting $U(2)$ representation has the form of a tensor product vector space describing the (uncoupled) anharmonic behavior exhibited by the constituent oscillators which often can be associated with particular local stretching and bending motions of the molecular framework. The interactions taking place between such ''local oscillators'' are a crucial aspect of intramolecular dynamics and can be partitioned into two broad categories depending upon whether they are diagonal or nondiagonal in the uncoupled (tensor product) basis. These essential characteristics can be incorporated into a model vibron Hamiltonian given by:

$$H = E_0 + \sum_{i=1}^{n} A_i C_i + \sum_{i\leqslant j}^{n} A_{ij} C_i C_j + \sum_{i<j}^{n} \lambda_{ij} M_{ij}, \tag{5}$$

where terms involving isolated Casimir operators, C_i, define an uncoupled set of n anharmonic oscillators (cf. Sec. IV A) while the product Casimir operators, $C_i C_j$, and Majorana operators, M_{ij}, describe the diagonal and nondiagonal interactions, respectively, which occur in the local basis.[67] In this article, we use the more convenient product Casimir operators, $C_i C_j$, instead of the operators C_{ij} of Iachello and Oss,[67] in order to isolate the explicit dependence on the product of vibrational quantum numbers $v_i v_j$. The effective zero-point energy is denoted as E_0, with the symbols A_i, A_{ij}, and λ_{ij} signifying adjustable parameters that reflect the detailed vibrational behavior of a particular system. Within the local tensor product representation, the matrix elements of operators C_i and $C_i C_j$ follow from:

$$\langle N_i, v_i | C_i | N_i, v_i' \rangle = \left(v_i - \frac{v_i^2}{N_i} \right) \delta v_i, v_i', \tag{6}$$

while the corresponding matrix elements for the Majorana operators, M_{ij}, can be formulated as:

$$\begin{aligned}\langle N_i,v_i;N_j,v_j|M_{ij}|N_i,v_i';N_j,v_j'\rangle &= \left[\left(1-\frac{v_j}{N_j}\right)(v_j+1)\left(1-\frac{v_i-1}{N_i}\right)v_i\right]^{1/2}\delta_{v_j,v_j'+1}\delta_{v_i,v_i'-1} \\ &+\left[\left(1-\frac{v_i}{N_i}\right)(v_i+1)\left(1-\frac{v_j-1}{N_j}\right)v_j\right]^{1/2} \\ &\times\delta_{v_i,v_i'+1}\delta_{v_j,v_j'-1}. \end{aligned} \tag{7}$$

The matrix elements in Eq. (7) have been given in a form that reduces to conventional normal mode coupling expressions in the harmonic limit (i.e., when $N_i\rightarrow\infty$).[65] The nondiagonal interactions introduced by the Majorana operators are found only to mix vibrational states having the same total number of quanta (viz. $v_i+v_j=$constant). This leads to a block diagonal representation of H in the local oscillator basis, where each block can be characterized by a unique multiplet label, V, derived from the sum of quantum numbers, $V=v_1+v_2+v_3$.[14,15] Such simplification greatly facilitates diagonalization of the vibron Hamiltonian to obtain the desired vibrational eigenvalues (i.e., fundamental frequencies and overtones) and their corresponding eigenvectors, with the latter expressed as an expansion over (uncoupled) tensor product basis states. Exhaustive attempts to incorporate other resonant interactions, including Fermi perturbations based upon integer multiples of the three fundamental vibrational frequencies, did not lead to statistically significant improvements in the quality of energy level analyses performed on either the ground or excited electronic manifolds of the S_2O system.

C. Franck–Condon factors and transition intensities

The algebraic evaluation of multidimensional Franck–Condon factors and associated vibronic transition intensities requires detailed knowledge of the vibrational eigenstates supported by two distinct potential surfaces. Such information can be obtained readily through least-squares adjustment of modeling parameters embodied in the appropriate vibron Hamiltonian for each electronic manifold so as to reproduce experimentally observed patterns of vibrational energy levels.[14,15] In particular, this procedure yields expressions for the corresponding vibrational eigenvectors in terms of the local anharmonic basis. The $U(2)$ Lie algebraic treatment of the nonlinear triatomic S_2O species entails three one-dimensional oscillators, leading to the uncoupled tensor product representation $|N_a,v_a;N_b,v_b;N_c,v_c\rangle\equiv|N_a,v_a\rangle\otimes|N_b,v_b\rangle\otimes|N_c,v_c\rangle$ where the subscripts *a*, *b*, and *c* affixed to quantum numbers signify the local S–O stretching, S–S stretching, and S–S–O bending degrees of freedom, respectively. Independent diagonalization of vibron Hamiltonians for the $\tilde{X}\ ^1A'$ and $\tilde{C}\ ^1A'$ states of S_2O provide explicit values for the vibrational expansion coefficients:

$$\begin{aligned}|\tilde{X};v_1,v_2,v_3\rangle &= \sum_{v_a,v_b,v_c} d_{v_a,v_b,v_c}^{v_1,v_2,v_3}\,|\tilde{X};v_a,v_b,v_c\rangle, \\ |\tilde{C};v_1',v_2',v_3'\rangle &= \sum_{v_a',v_b',v_c'} c_{v_a',v_b',v_c'}^{v_1',v_2',v_3'}\,|\tilde{C};v_a',v_b',v_c'\rangle, \end{aligned} \tag{8}$$

where the numerical subscripts appearing on vibrational quantum numbers signify the conventional mode ordering for a bent triatomic system and the N_i labels of the local basis have been dropped for notational convenience. Assuming that the transition-inducing electric dipole moment operator does not exhibit a significant dependence upon nuclear coordinates (i.e., the Condon approximation),[4] the probability or intensity, $I_{v_1'v_2'v_3'\rightarrow v_1v_2v_3}$, of a vibronic emission process connecting initial electronically-excited state $|\tilde{C};v_1',v_2',v_3'\rangle$ with final ground state $|\tilde{X};v_1,v_2,v_3\rangle$ is proportional to the corresponding Franck–Condon factor, $|T_{v_1'v_2'v_3'\rightarrow v_1v_2v_3}|^2$:

$$I_{v_1'v_2'v_3'\rightarrow v_1v_2v_3}\propto\nu^4|T_{v_1'v_2'v_3'\rightarrow v_1v_2v_3}|^2, \tag{9}$$

with the characteristic ν^4 frequency dependence stemming from the calibration of our fluorescence detection apparatus for constant radiant sensitivity. The Franck–Condon factor of Eq. (9) is defined by the square modulus of the corresponding vibrational overlap integral:[4]

$$T_{v_1'v_2'v_3'\rightarrow v_1v_2v_3}=\langle\tilde{X};v_1,v_2,v_3|\tilde{C};v_1',v_2',v_3'\rangle. \tag{10}$$

These overlap integrals are inherently multidimensional; however, the local anharmonic basis of the vibron model introduces both conceptual and practical simplifications. In particular, the calculation of $T_{v_1'v_2'v_3'\rightarrow v_1v_2v_3}$ can be recast by exploiting the eigenvector expansions of Eq. (8):

$$\begin{aligned}T_{v_1'v_2'v_3'\rightarrow v_1v_2v_3} &= \sum_{\substack{v_a',v_b',v_c' \\ v_a,v_b,v_c}} (d_{v_a,v_b,v_c}^{v_1,v_2,v_3})^*\ c_{v_a',v_b',v_c'}^{v_1',v_2',v_3'} \\ &\times\langle\tilde{X};v_a,v_b,v_c|\tilde{C};v_a',v_b',v_c'\rangle, \end{aligned} \tag{11}$$

where the tensor product nature of the uncoupled representation leads to a further partitioning into computationally-expedient products of one-dimensional integrals:[48]

$$\begin{aligned}&\langle\tilde{X};v_a,v_b,v_c|\tilde{C};v_a',v_b',v_c'\rangle \\ &=\langle\tilde{X};v_a|\tilde{C};v_a'\rangle\langle\tilde{X};v_b|\tilde{C};v_b'\rangle\langle\tilde{X};v_c|\tilde{C};v_c'\rangle. \end{aligned} \tag{12}$$

Furthermore, the intrinsic coordinates (viz. local internal coordinates) utilized by the vibron scheme permit changes in equilibrium geometry between the initial ($\tilde{C}\ ^1A'$) and final ($\tilde{X}\ ^1A'$) electronic states to be specified completely in terms of simple translational displacements,[3,20] thereby eliminating the complications (i.e., Duschinsky effect)[18] incurred during analogous normal mode treatments (which also neglect the influence of mechanical anharmonicity).

The local basis integrals of Eq. (12) entail the eigenstates of one-dimensional Morse (or Pöschl–Teller) potentials and can be evaluated by a variety of methods. Rather than resorting to a purely numerical procedure, the ensuing Franck–Condon calculations make use of an analytical formula[48,68] derived through perturbative correction of the analogous overlap expression for two harmonic oscillators characterized by different frequencies, $\omega(\omega')$, and concavities, $\alpha(\alpha')$, as well as relative spatial displacement, Δ:

$$\langle v|v'\rangle = \int_{-\infty}^{+\infty} \psi_v^*(\alpha;x)\psi_{v'}(\alpha';(x-\Delta))dx = \exp\left(\frac{-(\alpha\alpha'\Delta)^2}{2(\alpha^2+\alpha'^2)}\right)\left(\frac{\alpha\alpha' v!\, v'!}{2^{v+v'}}\frac{2}{\alpha^2+\alpha'^2}\right)^{1/2}$$
$$\times\left(\frac{1}{\alpha^2+\alpha'^2}\right)^{(v+v')/2}\sum_{l=0}^{\min\{v,v'\}}\frac{1}{l!\left(-\dfrac{(\alpha\alpha'\Delta)^2}{\alpha^2+\alpha'^2}\right)^l}\sum_{\substack{v\geqslant j\geqslant l\\ j=v \bmod 2}}\sum_{\substack{v'\geqslant j'\geqslant l\\ j'=v' \bmod 2}}$$
$$\times\frac{(\alpha^2-\alpha'^2)^{(v-j)/2}(\alpha'^2-\alpha^2)^{(v'-j')/2}}{(\alpha^2+\alpha'^2)^{(j+j')/2}}\frac{\alpha^j\alpha'^{j'}(\alpha'^2)^j(-\alpha^2)^{j'}(2\Delta)^{j+j'}}{\left(\dfrac{v-j}{2}\right)!\left(\dfrac{v'-j'}{2}\right)!(j-l)!(j'-l)!}, \tag{13}$$

with $\alpha=\sqrt{\mu\omega/\hbar}$ defining the concavity for an harmonic oscillator of reduced mass, μ, and frequency, ω. This expression can be adapted to approximate the one-dimensional overlap integrals for anharmonic (e.g., Morse-type) oscillators, with first-order perturbation theory yielding corrections for the concavity, $\alpha\,(\alpha')$, and displacement, Δ, of the form:

$$\alpha=\alpha_0(1-\xi v),\quad \alpha'=\alpha_0'(1-\xi' v'),$$
$$\Delta=\Delta_0-\eta v+\eta' v', \tag{14}$$

where the values of α_0, ξ, and η (α_0', ξ', and η') can be estimated from the corresponding Morse parameters β, ω_e, and $\omega_e x_e$ [β', ω_e', and $(\omega_e x_e)'$]:[48,68]

$$\alpha_0=\beta\sqrt{\frac{\omega_e}{2\omega_e x_e}},\quad \alpha_0'=\beta'\sqrt{\frac{\omega_e'}{2(\omega_e x_e)'}},$$
$$\xi=\frac{5\omega_e x_e}{6\omega_e},\quad \xi'=\frac{5(\omega_e x_e)'}{6\omega_e'}, \tag{15}$$
$$\eta=\frac{2\omega_e x_e}{\beta\omega_e},\quad \eta'=\frac{2(\omega_e x_e)'}{\beta'\omega_e'}.$$

Despite the simplicity introduced by the analytical formula of Eq. (13), the explicit determination of overlap parameters still represents a formidable task. For the present S_2O $\tilde{C}-\tilde{X}$ studies, detailed consideration of emission data obtained through excitation of the 0_0^0 origin band enabled the influence of Δ_0 and α_0 to be examined in isolation since the vibrationless $\tilde{C}\ ^1A'$ level is neither mixed by Majorana coupling nor affected by the values of ξ and η. Consequently, the displacement and concavity for each local oscillator (viz. Δ_0^a and α_0^a where $a=$ SO, SS, or SSO) could be quantified by analyzing the intensity envelopes of vibronic progressions involving the corresponding vibrational degree of freedom, with the perturbative estimates of ξ and η from Eq. (15) allowing a first-order calculation of dispersed fluorescence amplitudes for remaining excitation lines. An iterative, manual adjustment of the parameters α_0, ξ, η, and Δ_0 was performed subsequently, thereby obtaining a global fit for all observed emission intensities.

Since the uncoupled tensor product basis represents anharmonic oscillators associated with local internal coordinates, the translational displacement parameters, Δ_0^{SO}, Δ_0^{SS}, and Δ_0^{SSO}, yield detailed information on the change in equilibrium geometry which accompanies the electronic transition. Assuming bonds to lengthen (on average) with increasing vibrational energy content, the signs of Δ_0^{SO} and Δ_0^{SS} can be ascertained from the first-order anharmonic corrections of Eq. (14). In contrast, the sign of Δ_0^{SSO} remains ambiguous since it is related to the modification in triatomic bond angle. All displacement parameters are given in units of length; however, Δ_0^{SSO} can be converted to obtain the corresponding angular displacement:

$$\Delta_0^{SSO}=r\,\theta_{SSO}-r'\,\theta_{SSO}',\quad r=\frac{r_{SS}+r_{SO}}{2}, \tag{16}$$

where, in keeping with the notation introduced for our Franck–Condon emission analysis, the primed and unprimed parameters refer to the (initial) excited and (final) ground electronic states, respectively.

V. RESULTS AND DISCUSSION

A. Vibrational energies for the $\tilde{X}\ ^1A'$ ground state

The long vibronic progressions observed in S_2O $\tilde{C}-\tilde{X}$ dispersed fluorescence spectra provide an extensive ground state data set consisting of 240 distinct vibrational levels which span $\sim$14 000 cm^{-1} of internal energy within the $\tilde{X}\ ^1A'$ potential surface. The resulting vibrational term values are complied in Table I with the measurement precision for these quantities estimated to be better than ± 5 cm^{-1}. Initial attempts to reproduce such laboratory findings through use of a minimal $U(2)$ vibron Hamiltonian involving only the three linear, diagonal Casimir operators, C_κ where $\kappa=a,b,c$ signifying the local S–O stretching, S–S stretching, and S–S–O bending degrees of freedom, respectively, gave an unsatisfactory root-mean-square (rms) deviation between experiment and theory of $\sim$35 cm^{-1}. This discrepancy was reduced to $\sim$9 cm^{-1} by including the complete set of six quadratic forms, $C_\kappa C_{\kappa'}$; however, further improvement could not be achieved by incorporating nondiagonal (Majorana) interactions. Indeed, the same optimized algebraic parameters were obtained under various modeling conditions,

TABLE II. Optimized Hamiltonian parameters for the algebraic description of S_2O. Parameters derived from the least-squares regression of experimentally-measured vibrational level patterns are presented for the algebraic Hamiltonians used to describe the $\tilde{X}\ ^1A'$ and $\tilde{C}\ ^1A'$ electronic states of S_2O, with values in parentheses signifying the associated one standard deviation uncertainties. The unitless quantum number N_α, where $\alpha=a$, b, or c represents the local S–O stretching, S–S stretching, and S–S–O bending degrees of freedom, respectively, indicate the number of bound eigenstates in each local (anharmonic) oscillator comprising the uncoupled U(2) basis. While N_a and N_b embody the Morse parameters for the corresponding S–O and S–S diatomic units, the bending motion is characterized by $N_c = N_a + N_b$. All other tabulated quantities are expressed in wavenumbers (cm^{-1}) with the linear diagonal parameters, A_α, reflecting the local-mode harmonic frequencies.

Algebraic Parameter	$\tilde{X}\ ^1A'$ Surface	$\tilde{C}\ ^1A'$ Surface
N_a	187	187
N_b	255	158
N_c	439	345
A_a	1155.77(37)	904.4(92)
A_b	678.797(58)	534.7(10)
A_c	381.73(16)	264.7(20)
A_{aa}	1.654(68)	⋯
A_{ab}	7.06(15)	⋯
A_{ac}	−2.240(55)	⋯
A_{bb}	0.2490(38)	⋯
A_{bc}	−3.237(43)	⋯
A_{cc}	0.750(29)	⋯
A_{abb}	−1.486(18)	⋯
A_{bbc}	0.0683(25)	⋯
A_{abbb}	0.04705(66)	⋯
λ_{ab}	⋯	257.1(67)
λ_{bc}	⋯	−44.0(35)
rms deviation	5.7	3.2

including the incremental augmentation of preliminary analyses based upon the minimal algebraic framework and a selected subset of the $\tilde{X}\ ^1A'$ eigenstates.

The inability to reproduce vibrational term values quantitatively through use of a coupled $U(2)$ scheme incorporating the quadratic $C_\kappa C_{\kappa'}$ Casimir forms prompted a detailed search for any systematic behavior in the deviations between experiment and theory. The predictions of the vibron model were found to be least satisfactory for $\tilde{X}\ ^1A'$ eigenstates involving substantial excitation of all three vibrational modes. Comparison of residual patterns with the energy shifts produced by various algebraic operators suggested the introduction of selective cubic and quartic combinations, leading to a vibron Hamiltonian of the form:

$$\begin{aligned} H_{\tilde{X}} = & A_a C_a + A_b C_b + A_c C_c + A_{aa} C_a C_a \\ & + A_{ab} C_a C_b + A_{ac} C_a C_c + A_{bb} C_b C_b \\ & + A_{bc} C_b C_c + A_{cc} C_c C_c + A_{abb} C_a C_b C_b \\ & + A_{bbc} C_b C_b C_c + A_{abbb} C_a C_b C_b C_b . \end{aligned} \tag{17}$$

Least-squares adjustment of the modeling parameters in $H_{\tilde{X}}$ produced the optimized quantities presented in Table II, with the comparison of experimentally-measured and theoretically-predicted vibrational term values in Table I showing an rms deviation of 5.7 cm^{-1}.

The absence of nondiagonal (Majorana) interactions in the ground state algebraic Hamiltonian implies that the corresponding S_2O vibrational dynamics are well described by local stretching and bending modes which, although anharmonic in nature, remain essentially uncoupled for the set of 240 levels examined by our dispersed fluorescence studies. This assertion of orthogonal and local vibrational degrees of freedom over a span of internal energy in excess of 1.6 eV [viz. ~46% of the D_0^0(S–SO) dissociation limit][69] is remarkable, especially given theoretical predictions of other bound species within the $\tilde{X}\ ^1A'$ potential surface. The *ab initio* calculations of Fueno and Buenker[39] have indicated two other (bound) isomers of C_{2v} symmetry to exist, an open SOS chain (1.90 eV) and a closed $S_2O(R)$ ring (1.58 eV) where the values in parentheses denote relative energies measured with respect to the global SSO minimum. Barrier heights for the various S_2O isomerization channels have not been documented; however, the small changes in vibrational behavior uncovered by the present studies would tend to suggest that the SSO↔$S_2O(R)$ barrier crest resides at energies substantially in excess of 1.6 eV.

The uniform local dynamics exhibited by the $S_2O\,\tilde{X}\ ^1A'$ manifold stand in stark contrast to the substantially more complex behavior found in the isovalent SO_2 species. Dispersed fluorescence measurements by Yamanouchi and co-workers[70] have probed 311 levels within the $SO_2\,\tilde{X}\ ^1A_1$ potential surface, thereby accessing eigenstates which contain up to ~20 500 cm^{-1} of rovibrational energy [viz. ~45% of the D_0^0(OS–O) dissociation limit].[71] Recent algebraic analyses of these data by Sako and Yamanouchi[72] have demonstrated a pronounced change in ground state vibrational character to accompany increasing internal excitation. Successful modeling of normal mode behavior observed in low energy regimes required the introduction of strong nondiagonal Majorana coupling between the degenerate pair of local S–O stretching degrees of freedom. At higher energies, detailed examination of level patterns and vibrational wavefunctions revealed a gradual, yet progressive, uncoupling of the local oscillator basis with the form of the resulting normal-to-local mode transition paralleling theoretical predictions made for the analogous O_3 molecule.[73] Consequently, the vibrational dynamics of S_2O would seem to resemble those of SO_2 only in the limit of extreme vibrational excitation. Evidently, the unique mass combination, absence of structural symmetry elements, and related mismatch of local oscillator frequencies in the S_2O system precludes efficient interaction of the (local) vibron basis leading to ''normal modes'' of vibration that closely approximate their ''local mode'' counterparts.

B. Vibrational energies for the $\tilde{C}\ ^1A'$ excited state

The algebraic interpretation of energy level patterns in the $S_2O\ \tilde{C}\ ^1A'$ potential surface is hampered by the onset of rapid predissociation which takes place for internal energies in excess of ~1200 cm^{-1}.[32,41,44–46] Aside from limiting the

TABLE III. Vibrational term values for the $\tilde{C}\ ^1A'$ state of S_2O. Most vibrational energies for the $\tilde{C}\ ^1A'$ potential surface were extracted from high-resolution ($\leqslant 0.05\ cm^{-1}$) and medium-resolution ($\leqslant 0.18\ cm^{-1}$) laser–induced fluorescence (LIF) work performed in our laboratory under jet-cooled conditions (Ref. 46). Term values for levels possessing substantial excitation of the ν_3 bending mode (i.e., designated by the symbol †) were derived from the bulk-gas optical–optical double resonance (OODR) studies of Tsukiyama *et al.* (Ref. 42) as recalibrated by comparison both with our own measurements and those reported by Clouthier and Rutherford (Ref. 43). The calculated energies follow from diagonalization of an optimized vibron Hamiltonian for the electronically-excited state, hereby yielding the tabulated deviations from experimental values. The partial energy fit, with its subset of vibrational states selected in order to minimize predissociation effects (Ref. 46), provided the eigenfunctions used for Franck–Condon analyses.

$v_1\ v_2\ v_3$	Measured term energy	Residual (global fit)	Residual (partial fit)
0 0 1	253.78(60)	1.07	0.88
0 1 0	410.56(18)	0.58	0.82
0 0 2	506.0(11)	1.9	1.4
0 1 1	661.98(60)	−0.27	−0.04
0 0 3	758.3(11)†	4.2	3.5
0 2 0	817.33(18)	0.82	0.85
0 1 2	912.5(11)	−0.7	−0.6
0 0 4	1006.9(11)†	4.2	3.1
1 0 0	1033.88(60)	2.70	1.69
0 2 1	1066.90(60)	−1.41	−1.21
0 1 3	1161.3(11)†	−1.5	−1.5
0 3 0	1220.23(18)	0.64	−0.00
1 0 1	1285.6(11)	1.9	0.9
0 2 2	1315.2(11)	−3.6	−3.3
0 1 4	1408.3(20)†	−2.8	
1 1 0	1438.02(60)	1.29	1.37
0 3 1	1468.43(60)	−2.44	−2.72
1 0 2	1536.2(11)	1.3	0.2
0 4 0	1618.92(60)	−0.28	−2.05
1 1 1	1686.3(11)	−2.5	−2.31
1 2 0	1837.4(11)	−1.6	−0.8
0 4 1	1866.8(20)	−3.1	
1 1 2	1938.3(11)	−1.3	−0.9
0 5 0	2012.44(60)	−2.9	
1 3 0	2229.5(11)	−8.3	−7.3
0 5 1	2257.8(20)	−7.7	
0 6 0	2405.3(20)	−2.7	
0 6 1	2652.9(20)	−4.6	
0 7 0	2800.4(20)	3.1	
0 7 1	3044.9(20)	−1.1	
0 8 0	3182.8(20)	−0.2	
2 3 0	3242.3(20)	−5.2	
0 8 1	3428.0(20)	−3.1	
0 9 0	3565.1(20)	−0.2	
0 9 1	3812.0(20)	−0.5	
0 10 0	3945.6(20)	1.5	
0 9 2	4059.7(20)	1.1	
0 10 1	4189.7(20)	−0.8	
0 11 0	4320.5(20)	1.1	

scope of high-quality spectral information, this phenomenon introduces perturbations into the manifold of vibrational spacings (*vide infra*). As shown by the data compiled in Table III, a total of 39 experimental term values are available, providing access to $\tilde{C}\ ^1A'$ eigenstates which possess up to 2, 11, and 4 quanta of excitation, respectively, in the ν_1, ν_2, and ν_3 modes. While 35 of the tabulated band origins were derived from high-resolution ($\leqslant 0.05\ cm^{-1}$) and medium-resolution ($\leqslant 0.18\ cm^{-1}$) LIF studies performed in our laboratory under jet-cooled conditions,[46] the positions of the remaining four vibrational levels are based upon the bulk-gas OODR work of Tsukiyama, *et al.*,[42] which were recalibrated by comparison with our measurements as well as those reported by Clouthier and Rutherford.[43]

Careful inspection of Table III reveals a local perturbation in vibrational term values to occur for $\tilde{C}\ ^1A'$ eigenstates having 6–7 quanta of excitation in the ν_2 S–S stretching degree of freedom. This observation, as well as the mode specificity noted for the rates of nonradiative decay processes,[46,47] tends to corroborate the previous predissociation studies of Zhang, *et al.*,[46] which suggested on the basis of a rudimentary one-dimensional tunneling model that the $\tilde{C}\ ^1A'$ potential surface intersects a dissociative electronic manifold roughly 2400 cm^{-1} above the $\tilde{C}–\tilde{X}$ band origin. Since the present work focuses on Franck–Condon transitions for bound states, algebraic analyses were restricted to 22 low-lying vibronic features (viz. including levels up to the fourth multiplet, $V=4$) which are all situated well below the predicted barrier crest for predissociation. The parameters included in the vibron Hamiltonian were limited to those that could be determined satisfactorily by this subset of spectral data:

$$H_{\tilde{C}}=A_aC_a+A_bC_b+A_cC_c+\lambda_{ab}M_{ab}+\lambda_{bc}M_{bc}, \qquad (18)$$

and all vibrational energies were weighted by their corresponding uncertainties in the least-squares regression procedure. The optimized vibron parameters obtained from this analysis are compiled in Table II with the comparison of measured and calculated term values in Table III showing the resulting rms deviation to be 3.2 cm^{-1}. Nondiagonal Majorana coupling was found to be exceptionally strong between the S–O and S–S stretching degrees of freedom (cf. $\lambda_{ab}M_{ab}$ term in $H_{\tilde{C}}$) although less pronounced interactions could also be discerned between the local S–S stretching and S–S–O bending oscillators (cf. $\lambda_{bc}M_{bc}$ term in $H_{\tilde{C}}$). As demonstrated in the following section, this pervasive mixing of local vibrational character has a profound influence on $\tilde{C}\ ^1A'$ vibrational eigenfunctions and the accompanying $\tilde{C}–\tilde{X}$ Franck–Condon intensities.[48]

C. Franck–Condon factors and emission intensities for the $\tilde{C}–\tilde{X}$ transition

The algebraic Franck–Condon treatment outlined in Eqs. (8)–(12) provides a viable approach for disentangling the wealth of geometrical and dynamical information contained in vibronically-resolved emission spectra. More specifically, the expansion coefficients used to describe molecular eigenstates in the vibron basis [viz. $\{c^{v_1',v_2',v_3'}_{v_a',v_b',v_c'}\}$ and $\{d^{v_1,v_2,v_3}_{v_a,v_b,v_c}\}$ in Eq. (8)] reflect the distinct vibrational behavior supported by the individual potential surfaces. These quantities follow from the detailed simulation of observed energy level patterns,[14,15] with Table II presenting the optimal modeling parameters deduced for the S_2O $\tilde{X}\ ^1A'$ and $\tilde{C}\ ^1A'$ states through diagonalization of the corresponding $H_{\tilde{X}}$ and $H_{\tilde{C}}$ algebraic Hamiltonians [cf. Eqs. (17) and (18)]. In contrast, overlap integrals evaluated in the uncoupled $U(2)$ representation [i.e., $\langle\tilde{X};v_a,v_b,v_c|\tilde{C};v_a',v_b',v_c'\rangle$ in Eqs. (11) and

TABLE IV. Perturbative and structural parameters for Franck–Condon analyses of S_2O. Parameters employed for Franck–Condon calculations in the S_2O $\tilde{C}\ ^1A' - \tilde{X}\ ^1A'$ system are compiled for each anharmonic degree of freedom comprising the (local) uncoupled $U(2)$ basis. The quantity α_0 specifies potential curvature (concavity), while ξ and η represent (first-order) corrections for concavity and displacement, respectively, which are employed for the perturbative evaluation of Morse-type overlap integrals (Refs. 48,68). The translational displacements reflecting changes in equilibrium geometry upon $\pi^* \leftarrow \pi$ electronic transition are given by the tabulated Δ_0 parameters. The intrinsic properties of the Morse-type potential furnished initial guesses for α_0, ξ, and η; however, all quantities were varied manually in order to reproduce the experimentally-observed emission envelopes.

Parameter	S–O Stretching	S–O Stretching	S–S–O Bending
$\tilde{C}\ ^1A'$ Surface:			
$\alpha_0(\text{Å}^{-1})$	18.95	15.96	10.99
ξ	0.0044	0.0035	0.0024
η(Å)	0.0	0.00441	0.0067
$\tilde{X}\ ^1A'$ Surface:			
$\alpha_0(\text{Å}^{-1})$	18.95	15.8	9.35
ξ	0.0044	0.005	0.0024
η(Å)	0.0018	0.0089	0.030
Translational Displacement:			
Δ_0(Å)	0.024	0.283	0.073

(12)] reveal the changes in molecular structure incurred through electronic excitation.[48,68] As demonstrated by the results compiled in Table IV, the precise relationship between (local) anharmonic oscillators comprising the ground and excited states can be ascertained from the analysis of Franck–Condon intensities, thereby enabling the extraction of equilibrium geometries and related structural constants.

The translational displacement parameters of Table IV (viz., Δ_0^{SO}, Δ_0^{SS}, and Δ_0^{SSO}) afford a measure of the alterations in molecular structure which accompany the S_2O $\tilde{C}-\tilde{X}$ transition. Given the known minimum energy configuration of the ground state,[35–37] these algebraic results yield a proposed equilibrium geometry for the $\tilde{C}\ ^1A'$ surface which is summarized in Table V along with analogous information derived from previous studies.[44] As suggested by the pronounced and extensive nature of the ν_2 progressions observed in all emission spectra, the S–S distance is found to elongate substantially from the $\tilde{X}\ ^1A'$ value of 1.8845 to 2.168 Å. In contrast, only a slight increase in S–O bond length from 1.459 to 1.483 Å is induced by the $\pi^* \leftarrow \pi$ electron promotion. The linear Δ_0^{SSO} displacement can be converted into an angular change by means of Eq. (16), thereby suggesting a $\tilde{C}\ ^1A'$ equilibrium bond angle of either $\angle\text{SSO} = 106°$ or $\angle\text{SSO} = 110°$ depending upon the (indeterminate) sign of Δ_0^{SSO}. It must be emphasized that the meager bending progressions uncovered in our dispersed fluorescence experiments reflect, primarily, the small magnitude of Δ_0^{SSO}, with the prediction of a significant (8° or 12°) decrease in S–S–O angle upon $\tilde{C} \leftarrow \tilde{X}$ excitation stemming from the large concomitant increase in S–S bond length which leads to near cancellation of the two terms appearing in Eq. (16). Inertial constants derived from vibron parameters are in good accord with published $\tilde{C}\ ^1A'$ rotational constants[44,46] upon which prior structural analyses have been based.[44]

TABLE V. Equilibrium structures for the $\tilde{X}\ ^1A'$ and $\tilde{C}\ ^1A'$ states of S_2O. Parameters describing equilibrium molecular geometries are tabulated for the ground and excited electronic states of S_2O. While the $\tilde{X}\ ^1A'$ r_s-structure follows from the microwave and infrared work of Lindenmayer, *et al.* (Ref. 37), the absence of detailed isotopic substitution data precludes analogous treatment of the $\tilde{C}\ ^1A'$ potential surface. Consequently, the $\tilde{C}\ ^1A'$ geometry proposed by Hallin, Merer, and Milton (Ref. 44) is based upon an assumed S–O bond length of 1.50 Å and inertial constants deduced from $\tilde{C}\ ^1A' - \tilde{X}\ ^1A'$ rovibronic lines, with qualitative Franck–Condon arguments providing further corroboration. Our quantitative Franck–Condon analyses permit the extraction of a $\tilde{C}\ ^1A'$ equilibrium structure based solely on vibrational information, thereby yielding results in reasonable agreement with those inferred from rotational analyses.

Surface	Source	r_{so} (Å)	r_{ss} (Å)	∠SSO
$\tilde{X}\ ^1A'$	Lindenmayer *et al.*[a]	1.459	1.8845	118.08°
$\tilde{C}\ ^1A'$	Hallin, Merer and Milton[b]	1.50	2.14	109°
$\tilde{C}\ ^1A'$	Present work	1.483	2.168	106° or 110°

[a]Reference 39.
[b]Reference 46.

The influence of intramolecular dynamics on S_2O intensity patterns is both dramatic and profound. This can best be appreciated by considering the hypothetical case of purely ''local'' (i.e., uncoupled) vibrational behavior in *both* electronic manifolds. Under such circumstances, the changes in equilibrium geometry accompanying the $\pi^* \leftarrow \pi$ transition would still lead to extensive S–S stretching progressions where the number of minima observed in vibronically-resolved emission envelopes would reflect the nodal count along the S–S coordinate for the corresponding $\tilde{C}\ ^1A'$ vibrational wavefunction.[74] Consequently, dispersed fluorescence data derived from selective excitation of the 2_0^1 band in the $\tilde{C}-\tilde{X}$ absorption system would again be dominated by 2_ν^1 features which display a single minimum in the intensity envelope as depicted in Fig. 2(c). However, the distribution of Franck–Condon intensity for all related progressions originating from the same $\tilde{C}\ ^1A'$ $\upsilon_2 = 1$ level [e.g., the $1_1^0 2_\nu^1$ progression in Fig. 2(c)] would be predicted to exhibit identical shapes as modified by a constant scaling factor depending on the values of displacement parameters Δ_0^{SO} and Δ_0^{SSO}. Clearly, the experimental results obtained for S_2O do not comply with this simplistic interpretation.

Excluding data sets acquired through excitation of the vibrationless origin band [cf. Fig. 2(a)], the S_2O dispersed fluorescence spectra do not display the identical (progression-independent) intensity envelopes that would be predicted for purely ''local'' vibrational dynamics within the $\tilde{X}\ ^1A'$ and $\tilde{C}\ ^1A'$ manifolds. Aside from the disparate nodal patterns observed for the 2_ν^1 and $1_1^0 2_\nu^1$ features of Fig. 2(c), analogous behavior is found in the $2_\nu^{\nu'}$ and $2_\nu^{\nu'} 3_1^0$ progressions of Figs. 3 and 4 where $\nu' = 3$ and $\nu' = 4$, respectively. Of even greater significance is the complete alteration in nodal patterns obtained for the $1_0^1 2_\nu^0$ and $1_1^1 2_\nu^0$ bands of Fig. 2(b), an effect also exhibited by the $2_\nu^{\nu'}$ and $1_1^0 2_\nu^{\nu'}$ progressions in Figs. 3 and 4. The vibron model has identified these

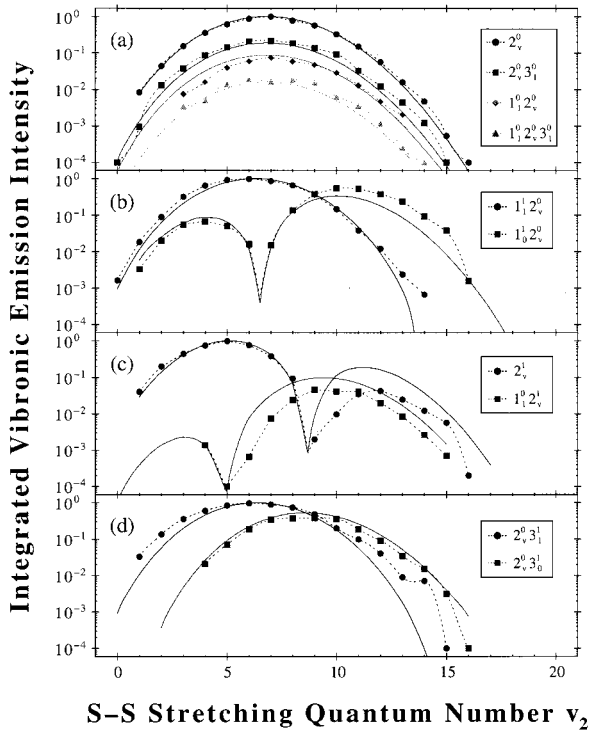

FIG. 2. Algebraic analyses of S_2O emission spectra. Vibron analyses of Franck–Condon intensities are presented for dispersed fluorescence data sets acquired through excitation of the (a) 0_0^0, (b) 1_0^1, (c) 2_0^1, and (d) 3_0^1 bands in the S_2O $\tilde{C}\ ^1A'-\tilde{X}\ ^1A'$ absorption system. The integrated spectral irradiance of single vibronic features is displayed as a function of the quantum number for S–S stretching, v_2, with the logarithmic scale serving to emphasize the overall shape and detailed nodal structure for each emission envelope. Solid curves follow from algebraic Franck–Condon calculations as outlined in the text, while the symbols connected with dashed lines represent experimental data. The highlighted $\tilde{C}\rightarrow\tilde{X}$ progressions are assigned nominally as: 2_v^0(●), $2_v^0 3_1^0$(■), $1_1^0 2_v^0$(◆), and $1_1^0 2_v^0 3_1^0$(▲) in panel (a): $1_1^1 2_v^0$(●) and $1_0^1 2_v^0$(■) in panel (b); 2_v^1(●) and $1_1^0 2_v^1$(■) in panel (c); and $2_v^0 3_1^1$(●) and $2_v^0 3_0^1$(■) in panel (d).

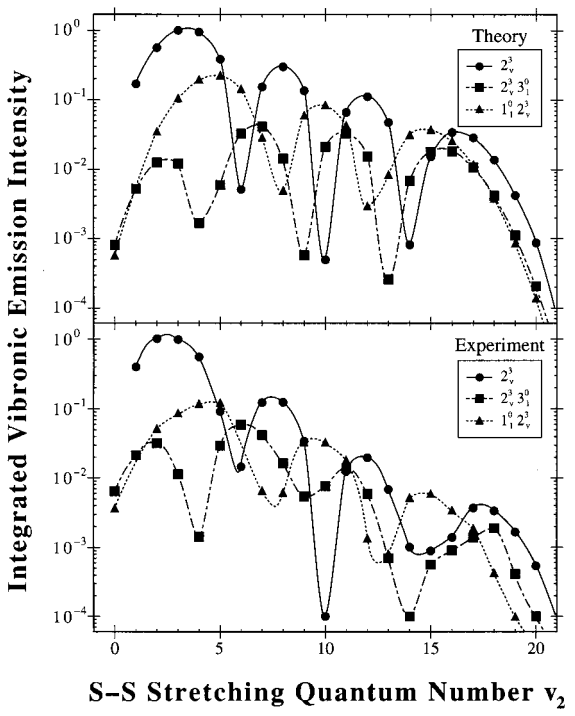

FIG. 3. Algebraic analysis of the 2^3 emission spectrum. Vibron analyses are presented for three progressions identified in dispersed fluorescence data stemming from selective excitation of the 2_0^3 band in the S_2O $\tilde{C}\ ^1A'-\tilde{X}\ ^1A'$ absorption system. Measured and calculated transition strengths are displayed as a function of the quantum number for S–S stretching, v_2, with the logarithmic scale serving to emphasize the overall shape and detailed nodal structure for each emission envelope. The theoretical Franck–Condon intensities in panel (a) are derived from the algebraic treatment outlined in the text while the experimental values in panel (b) represent the integrated spectral irradiance of single vibronic features. The three curves in each panel denote ground state progressions that are assigned nominally as 2_v^3(●), $2_v^3 3_1^0$(■), and $1_1^0 2_v^3$(▲).

effects as the signature of manifestly different vibrational behavior for the pertinent electronic manifolds. While algebraic analyses reveal the $\tilde{X}\ ^1A'$ ground state to be essentially local in nature, strong nondiagonal (Majorana) coupling within the electronically-excited $\tilde{C}\ ^1A'$ surface leads to pervasive mixing of vibrational character as expressed in the local oscillator basis. Consequently, the eigenstate nominally assigned to the $\tilde{C}\ ^1A'$ ''$1^1 2^0$'' level is found to involve an admixture of $\sim$21% ''$1^0 2^1$'' character as reflected by the expansion coefficients $c_{100}^{100}=-0.8884$, $c_{010}^{100}=0.4583$, and $c_{001}^{100}=0.0263$. In contrast, the local dynamics suggested for the $\tilde{X}\ ^1A'$ manifold imply that the corresponding $d_{v_a,v_b,v_c}^{v_1 v_2, v_3}$ expansion coefficients will vanish unless $v_a=v_1$, $v_b=v_2$, and $v_c=v_3$. Owing to the small magnitude of the Δ_0^{SO} translational displacement parameter, the overlap integrals evaluated in Eq. (11) will be negligible unless the number of quanta in the local S–O oscillator, v_a, is conserved. Franck–Condon factors for the $1_1^1 2_v^0$ transitions in Fig. 2(b) are thus dominated by contributions from the local ''$1^1 2^0$'' component and do not display the node ascribed to the local S–S stretching degree of freedom. Conversely, emission intensities for the accompanying $1_0^1 2_v^0$ progression are governed primarily by the ''$1^0 2^1$'' basis state and therefore display a single pronounced node. The removal of a ν_1 quantum during the $\tilde{C}\rightarrow\tilde{X}$ fluorescence process thus results in the appearance of an additional node within the ν_2 S–S stretching intensity envelope. In a similar fashion, Figs. 2(c), 3, and 4 demonstrate that emission features terminating on $\tilde{X}\ ^1A'$ levels which contain an additional ν_1 quantum (i.e., with respect to the initial $\tilde{C}\ ^1A'$ level) generally exhibit the concomitant loss of a node along the ν_2 coordinate. This is again a manifestation of nonlocality in the $\tilde{C}\ ^1A'$ state, where the nominal $1^m 2^n$ vibrational level contains significant ''$1^{m+1} 2^{n-1}$'' and ''$1^{m-1} 2^{n+1}$'' character.

While the quantitative simulation of dispersed fluorescence intensities can serve to validate predictions deduced from the algebraic treatment, it also furnishes a means to resolve ambiguities which arise from the restricted set of experimental measurements and the correspondingly limited number of well-determined vibron parameters. In particular, the model Hamiltonian used to describe vibrational dynamics of the electronically-excited potential surface [cf. Eq. (19)]

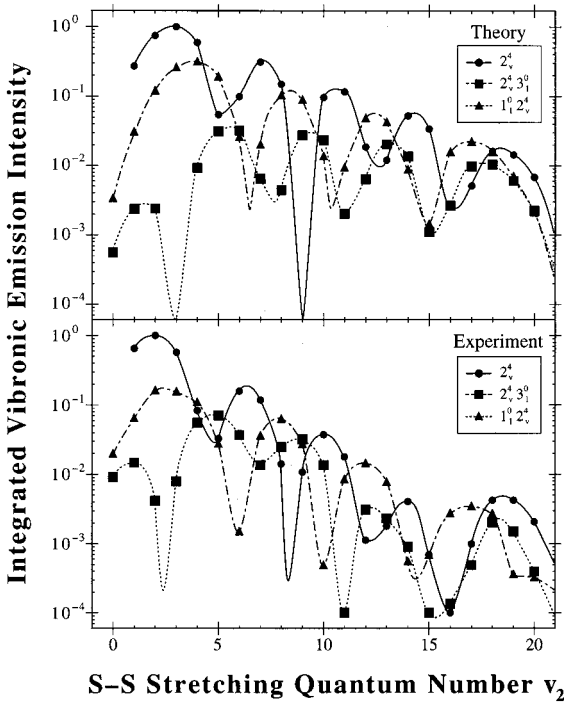

FIG. 4. Algebraic analysis of the 2^4 emission spectrum. Vibron analyses are presented for three progressions identified in dispersed fluorescence data stemming from selective excitation of the 2_0^4 band in the S_2O $\tilde{C}\ ^1A'-\tilde{X}\ ^1A'$ absorption system. Measured and calculated transition strengths are displayed as a function of the quantum number for S–S stretching, v_2, with the logarithmic scale serving to emphasize the overall shape and detailed nodal structure for each emission envelope. The theoretical Franck–Condon intensities in panel (a) are derived from the algebraic treatment outlined in the text while the experimental values in panel (b) represent the integrated spectral irradiance of single vibronic features. The three curves in each panel denote ground state progressions that are assigned nominally as 2_v^4(●), $2_v^4 3_1^0$(■), and $1_1^0 2_v^4$(▲).

has not incorporated Majorana interaction of the ν_a S–O stretching oscillator with the ν_c S–S–O bending basis although indirect mixing, as introduced through off-diagonal coupling of ν_a with ν_b and ν_b with ν_c, was found to be significant. This situation reflects the absence of observed $\tilde{C}\ ^1A'$ levels which simultaneously possess significant bending and S–O stretching character, thereby prohibiting accurate determination of a direct $\nu_a-\nu_c$ coupling term. The successful global analysis of vibronic emission envelopes demonstrated by Figs. 2–4 would tend to justify our neglect of such interactions; however, laboratory efforts designed to enhance the scope and quality of available data on $\tilde{C}\ ^1A'$ S_2O are underway.

The qualitative shapes of vibronically-resolved S_2O emission envelopes are reproduced successfully by the present algebraic treatment with minor discrepancies stemming primarily from the limited number of modeling parameters included in the $\tilde{C}\ ^1A'$ Hamiltonian. Quantitative comparisons of measured and predicted band intensities are favorable in most cases (cf. Table VI), a notable exception being found in the highest-lying portions of the extensive S–S stretching progressions accessed through excitation of the $2_0^{v'}(v' \geqslant 1)$ features. As shown in Figs. 2(c), 3, and 4, vibron analyses consistently overestimate the strength of transitions terminating on highly-excited ν_2 vibrational levels of the $\tilde{X}\ ^1A'$ potential surface. Since the ''experimentally-missing'' intensity does not manifest itself in other peaks or progressions comprising the recorded spectral data, modifications in vibrational dynamics, including intensity borrowing mechanisms ascribed to intramolecular (IVR) processes,[55] are unlikely to be responsible for observed discrepancies. An alternative explanation for this phenomenon can be found in non-Condon effects which arise from an explicit dependence of transition moment operators on nuclear (vibrational) degrees of freedom. The algebraic formalism provides a straightforward approach for performing intensity calculations that transcend limitations imposed by the canonical Condon approximation.[14] As highlighted in a forthcoming publication, substantial improvements can be achieved in the detailed simulation of S_2O dispersed fluorescence patterns by incorporating a transition dipole that scales with the S–S stretching coordinate.

VI. SUMMARY AND CONCLUSIONS

Fluorescence induced by selective excitation of individual vibronic bands in the jet-cooled S_2O $\tilde{C}\ ^1A' \leftarrow \tilde{X}\ ^1A'$ $(\pi^* \leftarrow \pi)$ absorption system has been dispersed under moderate spectral resolution with the resulting emission frequencies and intensities interpreted quantitatively through use of a novel algebraic scheme. In particular, our analyses exploit the unique capabilities afforded by a Lie algebraic description of molecular structure and dynamics, thereby establishing a comprehensive framework for the extraction of detailed vibrational information from spectroscopic data sets. The success of this approach builds upon the inherent simplicity, economy of parametrization, and coupled *anharmonic* nature of the underlying vibron Hamiltonian. As highlighted by the present treatment of vibronically-resolved emission spectra for the triatomic S_2O species, such features enable the facile evaluation of multidimensional Franck–Condon factors and related transition moment matrix elements.

The picture of S_2O vibrational dynamics that emerges from our algebraic analyses suggests radically different behavior for the ground and excited electronic states of the $\tilde{C}-\tilde{X}$ system. The positions of $\tilde{X}\ ^1A'$ vibrational levels over the observed 0–1.6 eV range of internal energy could be reproduced satisfactorily without incorporating nondiagonal mixing into the local anharmonic (vibron) basis, thereby implying that the ground potential surface supports exceptionally local and uncoupled vibrational motion. In contrast, the $\tilde{C}\ ^1A'$ manifold is distinguished by pervasive off-diagonal coupling between the local S–S stretching and S–O stretching degrees of freedom, as well as less pronounced interactions between the S–S stretching and bending coordinates. A quantifiable signature for such distinct intramolecular behavior has been identified in vibronically-resolved $\tilde{C}-\tilde{X}$ emission envelopes which exhibit nonintuitive nodal patterns that shift in a characteristic manner depending upon the selected excitation band. Structural parameters for the electronically-excited state have been deduced from the algebraic interpre-

TABLE VI. Emission intensities in the S_2O $\tilde{C}\ ^1A' \rightarrow \tilde{X}\ ^1A'$ transition. Experimental values represent the integrated and calibrated intensities measured for individual vibronic features by dispersing the $\tilde{C} \rightarrow \tilde{X}$ fluorescence from S_2O molecules entrained in a supersonic slit-jet environment. Calculated Franck–Condon signal strengths are based upon optimized algebraic descriptions for the $\tilde{X}\ ^1A'$ and $\tilde{C}\ ^1A'$ manifolds, with normalization selected so as to reproduce the maximum of emission observed in each spectrum. Data are presented for selected progressions identified upon excitation of the $^qR_0(1)$ rotational line in the 0_0^0 (origin), 1_0^1, 2_0^1, and 3_0^1 bands: (a) 2_ν^0, $2_\nu^0 3_1^0$, $1_1^0 2_\nu^0$, and $1_1^0 2_\nu^0 3_1^0$; (b) $1_0^1 2_\nu^0$ and $1_1^1 2_\nu^0$; (c) 2_ν^1 and $1_1^0 2_\nu^1$; and (d) the $2_\nu^0 3_1^1$ and $2_\nu^0 3_0^1$.

		2_ν^0		$2_\nu^0 3_1^0$		$1_1^0 2_\nu^0$		$1_1^0 2_\nu^0 3_1^0$	
(a)	v	Experimental intensity	Algebraic theory	Experimental intensity	Algebraic theory	Experimental intensity	Algebraic theory	Experimental intensity	Algebraic theory
	0			1.00×10^{-4}	1.04×10^{-4}				
	1	8.24×10^{-3}	6.96×10^{-3}	9.53×10^{-4}	1.30×10^{-3}				
	2	4.37×10^{-2}	4.05×10^{-2}	1.30×10^{-2}	7.54×10^{-3}	1.00×10^{-4}	3.54×10^{-3}	1.00×10^{-4}	6.59×10^{-4}
	3	1.52×10^{-1}	1.45×10^{-1}	3.76×10^{-2}	2.71×10^{-2}	7.44×10^{-3}	1.27×10^{-2}	3.50×10^{-3}	2.36×10^{-3}
	4	3.60×10^{-1}	3.62×10^{-1}	8.63×10^{-2}	6.73×10^{-2}	1.58×10^{-2}	3.14×10^{-2}	5.15×10^{-3}	5.83×10^{-3}
	5	6.12×10^{-1}	6.62×10^{-1}	1.42×10^{-1}	1.23×10^{-1}	3.92×10^{-2}	5.73×10^{-2}	1.41×10^{-2}	1.06×10^{-3}
	6	8.66×10^{-1}	9.23×10^{-1}	2.08×10^{-1}	1.71×10^{-1}	5.94×10^{-2}	7.95×10^{-2}	1.93×10^{-2}	1.47×10^{-2}
	7	1.00	1.00	2.17×10^{-1}	1.86×10^{-1}	7.39×10^{-2}	8.60×10^{-2}	1.65×10^{-2}	1.59×10^{-2}
	8	7.73×10^{-1}	8.59×10^{-1}	1.85×10^{-1}	1.59×10^{-1}	5.82×10^{-2}	7.34×10^{-2}	1.85×10^{-2}	1.36×10^{-2}
	9	5.70×10^{-1}	5.86×10^{-1}	1.36×10^{-1}	1.08×10^{-1}	4.63×10^{-2}	4.99×10^{-2}	1.56×10^{-2}	9.20×10^{-3}
	10	3.30×10^{-1}	3.19×10^{-1}	9.20×10^{-2}	5.89×10^{-2}	2.85×10^{-2}	2.70×10^{-2}	6.36×10^{-3}	4.98×10^{-3}
	11	1.50×10^{-1}	1.39×10^{-1}	3.29×10^{-2}	2.56×10^{-2}	1.29×10^{-2}	1.17×10^{-2}	3.64×10^{-3}	2.15×10^{-3}
	12	5.63×10^{-2}	4.79×10^{-2}	1.22×10^{-2}	8.81×10^{-3}	4.65×10^{-3}	4.02×10^{-3}	1.18×10^{-3}	7.38×10^{-4}
	13	1.58×10^{-2}	1.30×10^{-2}	4.41×10^{-3}	2.39×10^{-3}	2.05×10^{-3}	1.09×10^{-3}	2.58×10^{-4}	1.20×10^{-4}
	14	4.69×10^{-3}	2.75×10^{-3}	1.21×10^{-3}	5.05×10^{-4}	1.00×10^{-4}	2.29×10^{-4}	1.00×10^{-4}	4.19×10^{-5}
	15	5.39×10^{-4}	4.44×10^{-4}	1.00×10^{-4}	8.12×10^{-5}				
	16	1.00×10^{-4}	5.30×10^{-5}						
	17								

		$1_0^1 2_\nu^0$		$1_1^1 2_\nu^0$	
(b)	v	Experimental intensity	Algebraic theory	Experimental intensity	Algebraic theory
	0			1.62×10^{-3}	9.50×10^{-4}
	1	3.33×10^{-3}	5.81×10^{-3}	1.85×10^{-2}	1.12×10^{-2}
	2	2.02×10^{-2}	2.50×10^{-2}	8.95×10^{-2}	6.13×10^{-2}
	3	5.41×10^{-2}	6.04×10^{-2}	3.15×10^{-1}	2.05×10^{-1}
	4	6.65×10^{-2}	8.59×10^{-2}	6.40×10^{-1}	4.71×10^{-1}
	5	5.11×10^{-2}	6.41×10^{-2}	9.18×10^{-1}	7.85×10^{-1}
	6	1.61×10^{-2}	1.17×10^{-2}	9.80×10^{-1}	9.80×10^{-1}
	7	1.51×10^{-2}	1.27×10^{-2}	8.55×10^{-1}	9.31×10^{-1}
	8	1.35×10^{-1}	1.18×10^{-1}	6.51×10^{-1}	6.78×10^{-1}
	9	3.75×10^{-1}	2.63×10^{-1}	3.69×10^{-1}	3.76×10^{-1}
	10	5.45×10^{-1}	3.32×10^{-1}	1.45×10^{-1}	1.56×10^{-1}
	11	5.24×10^{-1}	2.85×10^{-1}	3.78×10^{-2}	4.66×10^{-2}
	12	3.78×10^{-1}	1.79×10^{-1}	1.21×10^{-2}	9.09×10^{-3}
	13	2.35×10^{-1}	8.45×10^{-2}	2.39×10^{-3}	8.75×10^{-4}
	14	9.20×10^{-2}	3.03×10^{-2}	6.66×10^{-4}	6.50×10^{-4}
	15	3.75×10^{-2}	8.25×10^{-3}	1.00×10^{-4}	2.71×10^{-5}
	16	1.60×10^{-3}	1.69×10^{-3}		
	17	1.00×10^{-4}	2.55×10^{-4}		
	18				

		2_ν^1		$1_1^0 2_\nu^1$	
(c)	v	Experimental intensity	Algebraic theory	Experimental intensity	Algebraic theory
	0				
	1	4.10×10^{-2}	2.92×10^{-2}		
	2	2.01×10^{-1}	1.42×10^{-1}		
	3	4.42×10^{-1}	4.08×10^{-1}		
	4	7.54×10^{-1}	7.71×10^{-1}	1.38×10^{-3}	1.34×10^{-3}
	5	9.82×10^{-1}	9.82×10^{-1}	1.00×10^{-4}	7.55×10^{-5}
	6	7.66×10^{-1}	8.26×10^{-1}	6.67×10^{-4}	7.61×10^{-3}
	7	3.83×10^{-1}	4.08×10^{-1}	7.49×10^{-3}	3.29×10^{-2}
	8	9.26×10^{-2}	7.04×10^{-2}	2.41×10^{-2}	6.94×10^{-2}
	9	2.00×10^{-3}	8.46×10^{-3}	4.62×10^{-2}	9.50×10^{-2}
	10	9.83×10^{-3}	1.13×10^{-1}	4.14×10^{-2}	9.33×10^{-2}
	11	3.48×10^{-2}	1.85×10^{-1}	4.09×10^{-2}	6.86×10^{-2}
	12	4.25×10^{-2}	1.61×10^{-1}	1.99×10^{-2}	3.87×10^{-2}

TABLE VI. (*Continued.*)

		2_v^1		$1_1^0 2_v^1$	
(c)	v	Experimental intensity	Algebraic theory	Experimental intensity	Algebraic theory
	13	2.49×10^{-2}	9.20×10^{-2}	8.36×10^{-3}	1.68×10^{-2}
	14	1.22×10^{-2}	3.76×10^{-2}	2.68×10^{-3}	5.66×10^{-3}
	15	5.68×10^{-3}	1.12×10^{-2}	7.01×10^{-4}	1.46×10^{-3}
	16	1.50×10^{-4}	2.47×10^{-3}		
	17				

		$2_v^0 3_1^1$		$2_v^0 3_0^1$	
(d)	v	Experimental intensity	Algebraic theory	Experimental intensity	Algebraic theory
	0	1.00×10^{-4}	8.80×10^{-4}		
	1	3.35×10^{-2}	1.04×10^{-2}		
	2	1.34×10^{-1}	5.78×10^{-2}		
	3	3.55×10^{-1}	1.95×10^{-1}		
	4	6.02×10^{-1}	4.54×10^{-1}	2.10×10^{-2}	2.63×10^{-2}
	5	8.48×10^{-1}	7.66×10^{-1}	7.16×10^{-2}	9.17×10^{-2}
	6	9.71×10^{-1}	9.71×10^{-1}	1.87×10^{-1}	2.19×10^{-1}
	7	8.92×10^{-1}	9.42×10^{-1}	3.35×10^{-1}	3.82×10^{-1}
	8	7.42×10^{-1}	7.04×10^{-1}	3.77×10^{-1}	5.04×10^{-1}
	9	4.81×10^{-1}	4.05×10^{-1}	3.81×10^{-1}	5.15×10^{-1}
	10	2.01×10^{-1}	1.77×10^{-1}	3.60×10^{-1}	4.13×10^{-1}
	11	1.00×10^{-1}	5.75×10^{-2}	1.86×10^{-1}	2.62×10^{-1}
	12	4.07×10^{-2}	1.31×10^{-2}	9.17×10^{-2}	1.32×10^{-1}
	13	9.07×10^{-3}	1.81×10^{-3}	3.48×10^{-2}	5.25×10^{-2}
	14	7.13×10^{-3}	9.63×10^{-5}	1.55×10^{-2}	1.64×10^{-2}
	15			3.09×10^{-3}	4.01×10^{-3}
	16				

tation of dispersed fluorescence spectra, yielding a predicted $\tilde{C}\ ^1A'$ equilibrium geometry which is in good accord with that inferred from previous measurements of rotational constants.[44]

The methodology introduced in this paper provides unique capabilities that can readily be extended and refined. Aside from obvious advantages afforded by the explicit incorporation of mechanical anharmonicity into the zero-order vibrational Hamiltonian, algebraic Franck–Condon analyses for polyatomic species can achieve exceptional computational efficiency owing to the separability that the underlying vibron basis introduces into an otherwise multidimensional problem. Moreover, the intrinsic coordinates (i.e., local internal coordinates) employed by this approach permit changes in equilibrium geometry between initial and final states to be specified completely in terms of simple translational displacements.[3,20] Consequently, the evaluation of requisite overlap integrals is not encumbered by the coordinate transformation difficulties (e.g., the Duschinsky effect)[18] that often plague analogous normal mode treatments. Most importantly, this scheme is robust in both concept and execution, permitting large molecular systems and complicated potential energy hypersurfaces to be addressed. Calculations that move beyond the Condon approximation, so as to include dependence of the transition moment operator on internal degrees of freedom, are in progress with a future publication demonstrating the substantial improvement between predicted and measured S_2O emission intensities (i.e., for high $\tilde{X}\ ^1A'$ energies) that can be obtained in this manner. Building upon known algebraic descriptions for the unbound (scattering) states of a Morse oscillator,[62] parallel efforts are underway to develop the theoretical apparatus needed to embrace quasibound and repulsive electronic states within the vibron framework, thereby setting the stage for detailed algebraic investigations of dissociative and associative chemical processes.

ACKNOWLEDGMENTS

This work was performed under the auspices of the NSF Experimental Physical Chemistry Program and supported in part by U.S. DOE Grant No. DE-FG02-91ER40608. P.H.V. gratefully acknowledges the Dreyfus Foundation for a Camille Dreyfus Teacher-Scholar Award and The Packard Foundation for support through a Packard Fellowship for Science and Engineering. The authors wish to thank Dr. P. Dupré (CNRS/MPI High Field Magnet Laboratory, Grenoble, France) for assistance in the acquisition/interpretation of preliminary S_2O data and Mr. M. Ibrahim (Department of Physics, Yale University) for assistance in the perturbative evaluation of Franck–Condon factors.

[1] G. Herzberg, *Molecular Spectra and Molecular Structure: I. Spectra of Diatomic Molecules* (Van Nostrand Reinhold, New York, 1950).
[2] G. Herzberg, *Molecular Spectra and Molecular Structure: III. Electronic Spectra and Electronic Structure of Polyatomic Molecules* (Van Nostrand Reinhold, New York, 1966).

[3] D. C. Moule, in *Vibrational Structure in Electronic Spectra: The Poly-Dimensional Franck–Condon Method, Vibrational Spectra and Structure: A Series of Advances*, edited by J. R. Durig (Elsevier Scientific, Amsterdam, 1977), p. 228.
[4] J. Franck, Trans. Faraday Soc. **21**, 536 (1925); E. U. Condon, Phys. Rev. **32**, 858 (1928); G. Herzberg and E. Teller, Z. Phys. Chem. Abt. B **2**, 410 (1933); E. U. Condon, Am. J. Phys. **15**, 365 (1947).
[5] J. Jortner, S. A. Rice, and R. M. Hochstrasser, Adv. Photochem. **7**, 149 (1969); K. F. Freed, Acc. Chem. Res. **11**, 74 (1978); Y. Fujimura and T. Nakajima, Chem. Phys. **38**, 89 (1979).
[6] K. F. Freed, in *Energy Dependence of Electronic Relaxation Processes in Polyatomic Molecules, Radiationless Processes in Molecules and Condensed Phases*, edited by K. F. Fong (Springer-Verlag, Heidelberg, 1976), p. 23.
[7] M. J. Berry, Chem. Phys. Lett. **29**, 329 (1974); Y. B. Band and K. F. Freed, J. Chem. Phys. **63**, 3382 (1975); K. F. Freed and Y. B. Band, Excited States **3**, 109 (1977).
[8] K. F. Freed, M. D. Morse, and Y. B. Band, Faraday Discuss. Chem. Soc. **67**, 297 (1979); O. Atabek and R. Lefebvre, Chem. Phys. **23**, 51 (1977).
[9] R. Schinke, *Photodissociation Dynamics: Spectroscopy and Fragmentation of Small Polyatomic Molecules* (Cambridge University Press, Cambridge, 1993).
[10] F. H. Mies, J. Chem. Phys. **51**, 787 (1969); **51**, 797 (1969); A. E. Orel and W. H. Miller, *ibid.* **73**, 241 (1980); P. S. Julienne, Phys. Rev. A **26**, 3299 (1982).
[11] R. A. Marcus and N. Sutin, Biochim. Biophys. Acta **811**, 265 (1985); R. A. Marcus, Adv. Chem. Phys. **106**, 1 (1999).
[12] G. C. Schatz and J. Ross, J. Chem. Phys. **66**, 1021 (1977); **66**, 1037 (1977); D. J. Zvijac and J. Ross, *ibid.* **68**, 4468 (1978); C. L. Vila, J. L. Kinsey, J. Ross, and G. C. Schatz, *ibid.* **70**, 2414 (1979); B. C. Eu, Mol. Phys. **31**, 1261 (1976); B. W. Spath and W. H. Miller, Chem. Phys. Lett. **262**, 486 (1996).
[13] J. W. Gadzuk, in *Fundamental Excitations in Solids Pertinent to Desorption Induced by Electronic Transitions, Desorption Induced by Electronic Transitions: DIET I*, edited by N. H. Tolk, M. M. Traum, J. C. Tully, and T. E. Madey (Springer-Verlag, Berlin, 1983), p. 4; R. Gomer, in *Mechanisms of Electron-Stimulated Desorption, Desorption Induced by Electronic Transitions: DIET I*, edited by N. H. Tolk, M. M. Traum, J. C. Tully, and T. E. Madey (Springer-Verlag, Berlin, 1983), p. 40; E. B. Stechel, in *Time Dependent Theory of Electronic Structure and Nuclear Dynamics in DIET, Desorption Induced by Electronic Transitions: DIET II*, edited by W. Brenig and D. Menzel (Springer-Verlag, Berlin, 1985), p. 32.
[14] F. Iachello and R. D. Levine, *Algebraic Theory of Molecules* (Oxford University Press, New York, 1995).
[15] S. Oss, Adv. Chem. Phys. **93**, 455 (1996).
[16] J. Tellinghuisen, Adv. Chem. Phys. **60**, 299 (1985).
[17] I. Özkan, J. Mol. Spectrosc. **139**, 147 (1990).
[18] F. Duschinsky, Acta Physicochim. URSS **7**, 551 (1937).
[19] E. V. Doktorov, I. A. Malkin, and V. I. Man'ko, J. Mol. Spectrosc. **56**, 1 (1975); Chem. Phys. Lett. **46**, 183 (1977); J. Mol. Spectrosc. **64**, 302 (1977); *ibid.* **77**, 178 (1979); K. Nishikawa, Int. J. Quantum Chem. **XII**, 859 (1977); D. Gruner and P. Brumer, Chem. Phys. Lett. **138**, 310 (1987); L. S. Cederbaum and W. Domcke, J. Chem. Phys. **64**, 603 (1976); **64**, 612 (1976); W. Domcke, L. S. Cederbaum, H. Köppel, and W. von Niessen, Mol. Phys. **34**, 1759 (1977); M. Roche, Chem. Phys. Lett. **168**, 556 (1990).
[20] T. E. Sharp and H. M. Rosenstock, J. Chem. Phys. **41**, 3453 (1964); R. Botter, V. H. Dibeler, J. A. Walker, and H. M. Rosenstock, *ibid.* **44**, 1271 (1966); R. Botter and H. M. Rosenstock, Adv. Mass Spectrom. **4**, 579 (1968); H. M. Rosenstock, Int. J. Mass Spectrom. Ion Phys. **7**, 33 (1971); H. Kupka and P. H. Cribb, J. Chem. Phys. **85**, 1303 (1986); R. Islampour, M. Dehistani, and S. H. Lin, J. Mol. Spectrosc. **194**, 179 (1999).
[21] T. R. Faulkner and F. S. Richardson, J. Chem. Phys. **70**, 1201 (1979); K. C. Kulander, *ibid.* **71**, 2736 (1979); J. Subbi, Chem. Phys. **122**, 157 (1988).
[22] K.-M. Chen and C.-C. Pei, Chem. Phys. Lett. **165**, 523 (1990); J. Mol. Spectrosc. **140**, 401 (1990).
[23] D. M. Burland and G. W. Robinson, J. Chem. Phys. **51**, 4548 (1969).
[24] D. Kusnezov, J. Chem. Phys. **101**, 2289 (1994).
[25] R. Bijker, R. D. Amado, and D. A. Sparrow, Phys. Rev. A **33**, 871 (1986); R. Bijker and R. D. Amado, *ibid.* **34**, 71 (1986); **37**, 1425 (1988); A. Mengoni and T. Shirai, J. Mol. Spectrosc. **12**, 246 (1993).
[26] J. L. Dunham, Phys. Rev. **41**, 713 (1932); **41**, 721 (1932).
[27] M. E. Kellman, Annu. Rev. Phys. Chem. **46**, 395 (1995).
[28] O. S. van Roosmalen, I. Benjamin, and R. D. Levine, J. Chem. Phys. **81**, 5986 (1984); R. D. Levine and J. L. Kinsey, J. Phys. Chem. **90**, 3653 (1986).
[29] P. W. Schenk, Z. Anorg. Allg. Chem. **211**, 150 (1933).
[30] D. J. Meschi and R. J. Myers, J. Am. Chem. Soc. **78**, 6220 (1956).
[31] D. J. Meschi and R. J. Myers, J. Mol. Spectrosc. **3**, 405 (1959).
[32] A. V. Jones, J. Chem. Phys. **18**, 1263 (1950).
[33] A. R. V. Murthy, Indian Acad. Sci. **36**, 388 (1952); B. S. Rao, Indian Acad. Sci. **10**, 491 (1939).
[34] R. L. Cook, J. Mol. Spectrosc. **46**, 276 (1973); E. Tiemann, J. Hoeft, F. J. Lovas, and D. R. Johnson, J. Chem. Phys. **60**, 5000 (1974).
[35] U. Blukis and R. J. Myers, J. Phys. Chem. **69**, 1154 (1965).
[36] A. G. Hopkins, S. Y. Tang, and C. W. Brown, J. Am. Chem. Soc. **95**, 3486 (1973).
[37] J. Lindenmayer and H. Jones, J. Mol. Spectrosc. **112**, 71 (1985); J. Lindenmayer, *ibid.* **116**, 315 (1986); J. Lindenmayer, H. D. Rudolph, and H. Jones, *ibid.* **119**, 56 (1986).
[38] R. O. Jones, Chem. Phys. Lett. **125**, 221 (1986).
[39] T. Fueno and R. J. Buenker, Theor. Chim. Acta **73**, 123 (1988).
[40] H. Cordes, Z. Phys. **105**, 251 (1937); E. Kondrat'eva and V. Kondrat'eva, J. Phys. Chem. USSR **14**, 1528 (1940); J. O. P. McBride, Ph.D. thesis, McMaster University, 1968.
[41] G. Lakshminarayana, J. Mol. Spectrosc. **55**, 141 (1975).
[42] K. Tsukiyama, D. Kobayashi, K. Obi, and I. Tanaka, Chem. Phys. **84**, 337 (1984).
[43] D. J. Clouthier and M. L. Rutherford, Chem. Phys. **127**, 189 (1988).
[44] K.-E. J. Hallin, A. J. Merer, and D. J. Milton, Can. J. Phys. **55**, 1858 (1977).
[45] C. L. Chiu, P. C. Sung, and L. D. Chen, J. Mol. Spectrosc. **94**, 343 (1982).
[46] Q. Zhang, P. Dupré, B. Grzybowski, and P. H. Vaccaro, J. Chem. Phys. **103**, 67 (1995).
[47] Q. Zhang, Ph.D. thesis, Yale University, 1996.
[48] T. Müller, P. Dupré, P. H. Vaccaro, F. Pérez-Bernal, M. Ibrahim, and F. Iachello, Chem. Phys. Lett. **292**, 243 (1998).
[49] S. Gerstenkorn and P. Luc, Rev. Phys. Appl. **14**, 791 (1979); **14**, 791 (1979).
[50] P. W. Schenk and R. Steudel, in *Oxides of Sulfur, Inorganic Sulphur Chemistry*, edited by G. Nickless (Elsevier, Amsterdam, 1968), p. 10.; A. R. Vasudeva-Muthy, N. Kutty, and D. K. Sharma, Int. J. Sulfur Chem. B. **6**, 161 (1971).
[51] *CRC Handbook of Chemistry and Physics* (CRC, Boca Raton, FL, 1998-1999).
[52] T. Müller and P. H. Vaccaro, Rev. Sci. Instrum. **69**, 406 (1998).
[53] Photomultiplier Tubes Catalog (Hamamatsu Photonics K. K., Japan, 1994), p. 81.
[54] T. Müller, P. D. Dupré, and P. H. Vaccaro (unpublished).
[55] D. J. Nesbitt and R. W. Field, J. Phys. Chem. **100**, 12735 (1996).
[56] S. Lie, *Vorlesungen Über Continuerliche Gruppen*, edited by G. Scheffers (Teubner, Leipzig, 1893).
[57] F. Iachello, in *Proceedings of Int. Conf. on Nuclear Structure and Spectroscopy, Amsterdam, 1974*, edited by H. P. Blok and A. E. L. Dieperink (Scholar's Press), p. 163; A. Arima and F. Iachello, Phys. Rev. Lett. **35**, 1069 (1975); Ann. Phys. (Leipzig) **99**, 253 (1976).
[58] F. Iachello and A. Arima, *The Interacting Boson Model* (Cambridge, New York, 1987).
[59] F. Iachello, Chem. Phys. Lett. **78**, 581 (1981); F. Iachello and R. D. Levine, J. Chem. Phys. **77**, 3046 (1982); O. S. van Roosmalen, A. E. L. Dieperink, and F. Iachello, Chem. Phys. Lett. **85**, 32 (1982); O. S. van Roosmalen, F. Iachello, R. D. Levine, and A. E. L. Dieperink, J. Chem. Phys. **79**, 2515 (1983).
[60] P. Cordero and S. Hojman, Lett. Nuovo Cimento **4**, 1123 (1970); R. D. Levine and C. E. Wulfman, Chem. Phys. Lett. **60**, 372 (1979); M. Berrondo and A. Palma, J. Phys. A **13**, 773 (1980).
[61] Y. Alhassid, F. Gürsey, and F. Iachello, Chem. Phys. Lett. **99**, 27 (1983).
[62] Y. Alhassid, F. Gürsey, and F. Iachello, Ann. Phys. (N.Y.) **148**, 346 (1983).
[63] F. Iachello and S. Oss, Chem. Phys. Lett. **205**, 285 (1993).
[64] F. Iachello and S. Oss, J. Chem. Phys. **104**, 6956 (1996).
[65] A. Frank, R. Lemus, F. Bijker, F. Pérez-Bernal, and J. M. Arias, Ann. Phys. (Leipzig) **252**, 211 (1996).
[66] F. Pérez-Bernal, J. M. Arias, A. Frank, R. Lemus, and R. Bijker, J. Mol. Spectrosc. **184**, 1 (1997).

[67] F. Iachello and S. Oss, Phys. Rev. Lett. **66**, 2976 (1991).
[68] F. Iachello and M. Ibrahim, J. Phys. Chem. A **102**, 9427 (1998).
[69] J. Berkowitz, J. H. D. Eland, and E. H. Appelman, J. Chem. Phys. **66**, 2183 (1977).
[70] K. Yamanouchi, S. Takeuchi, and S. Tsuchiya, J. Chem. Phys. **92**, 4044 (1990).
[71] H. Okabe, J. Am. Chem. Soc. **93**, 7095 (1971).
[72] T. Sako and K. Yamanouchi, Chem. Phys. Lett. **264**, 403 (1997).
[73] M. E. Kellman, J. Chem. Phys. **83**, 3843 (1985); M. J. Davis and E. J. Heller, *ibid.* **75**, 246 (1981).
[74] J. B. Coon, R. E. DeWames, and C. M. Loyd, J. Mol. Spectrosc. **8**, 285 (1962).